TEAD1 is crucial for myelination, Remak bundles and functional regeneration of peripheral nerves

Matthew Grove[1], Hyukmin Kim[1], Shuhuan Pang[1], José Paz Amaya[2], Guoqing Hu[3], Jiliang Zhou[3], Michel Lemay[2], and Young-Jin Son[1]*

[1]Department of Neural Sciences, Shriners Hospitals Pediatric Research Center, Lewis Katz School of Medicine, Temple University, Philadelphia, PA 19140

[2]Department of Bioengineering, Temple University, Philadelphia, PA 19122, USA

[3]Department of Pharmacology & Toxicology, Medical College of Georgia, Augusta University, Augusta, GA

* Corresponding author: yson@temple.edu

ABSTRACT

The hippo pathway transcriptional effectors, YAP/TAZ, are crucial for Schwann cells (SCs) to myelinate axons but the partner transcription factor remains undetermined. Here, using conditional and inducible knockout mice, we report that TEAD1 is essential for SCs to develop, grow, and regenerate myelin sheaths. TEAD1/2/3/4 are all present in SCs, but YAP/TAZ strongly favors TEAD1. It promotes myelination by both positively and negatively regulating SC proliferation, enabling Krox20/Egr2 to upregulate myelin proteins, and upregulating the cholesterol biosynthetic enzymes FDPS and IDI1. We also show stage-dependent redundancy of TEAD1 and that non-myelinating SCs have a unique requirement for TEAD1 to enwrap nociceptive axons in Remak bundles. Our findings establish TEAD1 as a crucial partner of YAP/TAZ in developmental myelination and functional nerve regeneration and as a novel transcription factor regulating Remak bundle integrity.

KEYWORDS

YAP, TAZ, Hippo signaling, TEAD, myelin, Krox20, Egr2, radial sorting, peripheral neuropathy, Nerve injury, Remak Schwann cells, c fibers

INTRODUCTION

In the mammalian peripheral nervous system, all motor and sensory axons are associated with Schwann cells (SCs). Axons larger than 1μm diameter are enveloped by myelinating SCs that form multilamellar myelin sheaths with a thickness proportional to axon caliber (Jessen and Mirsky, 2005; Salzer, 2015). Axons smaller than 1μm diameter, the unmyelinated nociceptors (i.e., C-fibers), are organized in clusters called Remak bundles, in which each C-fiber is ensheathed by a cytoplasmic pocket formed by non-myelinating SCs, also known as Remak SCs (Beirowski et al., 2014; Harty and Monk, 2017). Both myelinating and non-myelinating SCs provide metabolic and functional support essential for structural and functional integrity of peripheral nerves. Failure to initiate or maintain proper axon-SC association may lead to life-threatening paralysis and peripheral neuropathy (Scherer and Wrabetz, 2008). Myelinating SCs form and maintain myelin via a set of key transcription factors (TFs) and regulators (Bremer et

54 al., 2011; Decker et al., 2006; Finzsch et al., 2010; He et al., 2010; Jaegle et al., 2003; Kao et al.,
55 2009; Le et al., 2005b). However, the transcriptional regulation of myelinating SCs remains
56 incompletely understood, and that of non-myelinating SCs is largely unknown (Harty and Monk,
57 2017).

58 Recent mouse genetic studies surprisingly revealed that YAP (Yes-associated protein)
59 and its paralogue, TAZ (Transcriptional coactivator with PDZ-binding motif), which are potent
60 oncoproteins and transcriptional regulators in the Hippo signaling pathway, play crucial roles in
61 developing, maintaining, and regenerating myelination of peripheral nerves. Both YAP and TAZ
62 (YAP/TAZ) are expressed initially in all immature SCs and then selectively in myelinating SCs
63 (Grove et al., 2017). The processes for which they are required include: timely sorting of large
64 axons and associated SC proliferation (Grove et al., 2017; Poitelon et al., 2016); initiation of SC
65 differentiation or myelination (Deng et al., 2017; Grove et al., 2017); myelin maintenance in
66 adults (Grove et al., 2017); and remyelination following nerve injury (Grove et al., 2020;
67 Jeanette et al., 2021). YAP/TAZ initiate and maintain myelination in part by upregulating
68 Krox20 (a.k.a., Egr2) (Grove et al., 2017; Lopez-Anido et al., 2016), which is widely recognized
69 as the master TF promoting peripheral myelination. Krox20 is required to initiate myelination,
70 maintain adult myelin (Decker et al., 2006; Topilko et al., 1994), and likely to promote myelin
71 sheath growth (Le et al., 2005a). It acts through direct transcriptional upregulation of myelin
72 proteins and membrane lipids (Jang et al., 2010; Jang and Svaren, 2009; LeBlanc et al., 2006).

73 YAP/TAZ are transcriptional co-activators that contain a transcriptional activation
74 domain, but no DNA binding domain. They regulate gene expression by binding to partner TFs,
75 typically members of the TEA domain family (TEAD1-4) (Zheng and Pan, 2019). Conversely,
76 TEADs on their own are unable to activate or repress transcription (Xiao et al., 1991) and require
77 the help of co-factors such as YAP/TAZ to act (Currey et al., 2021). Partner TFs such as TEADs
78 are required to maintain YAP/TAZ in the nucleus, which keeps them transcriptionally active
79 (Diepenbruck et al., 2014; Kim et al., 2020; Kofler et al., 2018; Yao et al., 2018). Transcript data
80 indicates that SCs express all four TEADs and that their expression peaks at different times
81 during development (Gerber et al., 2021). Moreover, TEAD1-4 show unique, redundant, and/or
82 opposing roles in regulating proliferation and differentiation of various cell types; these roles can
83 also change as a function of developmental stage (Currey et al., 2021; He et al., 2018; Holden
84 and Cunningham, 2018; Mukhtar et al., 2020). It remains to be elucidated how and which

85 TEAD(s) in SCs mediate transcriptional regulation of YAP/TAZ for the development,
86 homeostasis, and/or regeneration of myelination.
87 In some cells, TEAD1 serves as the main partner TEAD and plays non-redundant roles
88 (Liu et al., 2019; Wen et al., 2019). In SCs, ChiP, co-IP, and transcription assays have
89 consistently indicated that TEAD1 associates with YAP/TAZ for upregulating myelin proteins
90 (Fernando et al., 2016; Grove et al., 2017; Lopez-Anido et al., 2016; Lopez-Anido et al., 2015).
91 Notably, unlike YAP/TAZ, TEAD1 is expressed in all SC nuclei (Grove et al., 2017), suggesting
92 that, independently of YAP/TAZ, TEAD1 plays an unknown role in non-myelinating SCs. In this
93 study, we generated conditional and inducible knockout mice lacking TEAD1 in SCs to
94 investigate the roles of TEAD1 in myelinating and non-myelinating SCs. We found that TEAD1
95 is uniquely required for myelinating SCs to initiate, grow and regenerate myelination, and for
96 non-myelinating SCs to enwrap C-fibers in Remak bundles during development and
97 homeostasis. We also uncovered the mechanistic basis of the non-redundancy of TEAD1 and
98 found that YAP/TAZ-TEAD1 promotes myelination by dually regulating SC proliferation, by
99 enabling induced Krox20 to upregulate myelin proteins and by upregulating cholesterol
100 biosynthetic enzymes. Additional results suggest that other TEADs may play redundant and
101 opposing roles in a stage-dependent manner.
102
103 **RESULTS**
104
105 **Multiple TEADs are expressed in Schwann cells of WT, *Tead1* cKO and iKO mice**
106 To investigate the roles of SC TEAD1 in developing nerves, we conditionally ablated
107 *Tead1* by crossing *Tead1*$^{fl/fl}$ mice (Wen et al., 2017) with mice carrying *Mpz*-Cre, which is active
108 from E13.5 in SCs (Feltri et al., 1999). To investigate the roles of TEAD1 in maintaining and
109 regenerating nerves in adults, we inducibly inactivated SC *Tead1* by crossing *Tead1*$^{fl/fl}$ mice with
110 mice carrying a tamoxifen-inducible *Plp*-CreER (Leone et al., 2003). Immunostaining of P22
111 WT and *Mpz-Cre;Tead1*$^{fl/fl}$ (hereafter *Tead1* cKO) sciatic nerves (SNs) showed that TEAD1 was
112 expressed in the nuclei of 100% of WT SCs and was undetectable in >97% *Tead1* cKO SCs
113 (Figure 1A). Immunostaining of WT and *Plp* -CreER*; Tead1*$^{fl/fl}$ (hereafter *Tead1* iKO) SNs after
114 tamoxifen treatment showed that TEAD1 was also present in 100% of SC nuclei in both intact
115 and regenerating nerves of adult WT mice and was deleted in almost all *Tead1* iKO SCs (Figure

116 1B, 1C). The specificity of the TEAD1 immunostaining and highly efficient deletion were
117 further confirmed by Western blotting (Figure 1D). These results suggest potential roles for
118 TEAD1 in both myelinating and non-myelinating SCs during development, maintenance and
119 after nerve injury.
120 To investigate the expression of other TEADs in WT, *Tead1* cKO and *Tead1* iKO SCs,
121 we used antibodies to TEAD2, 3 and 4, and a pan-TEAD antibody marketed to recognize all four
122 TEADs (TEAD1/2/3/4). Western blot analysis of SN lysates showed that anti-TEAD3 and anti-
123 pan TEAD both revealed a main ~ 50kD band that was decreased in *Tead1* cKO (Figure 1D).
124 The pan-TEAD antibody may therefore bind preferentially to TEAD3. Anti-TEAD4 recognized
125 three bands in WT and showed that the two faster-migrating bands were decreased in *Tead1* cKO
126 (Figure 1D). Anti-TEAD2 recognized a band of ~65 kD in *Tead1* cKO that was barely detectable
127 in WT lysates. This band corresponded to the size of TEAD2 reported in other cell types
128 (Beverdam et al., 2013). We also found that the ~65 kD band was present early postnatally, but
129 rapidly diminished with age (data not shown), consistent with previous transcript data from
130 mouse SCs (Gerber et al., 2021). Therefore, the expression of TEAD2-4 was altered in *Tead1*
131 cKO, confirming the specificity of the antibodies and their expression in SCs. Of these anti-
132 TEAD antibodies, only anti-pan TEAD functioned effectively for immunofluorescence staining,
133 verifying the presence of other TEADs in SC nuclei in both intact (Figure 1E) and injured WT
134 and *Tead1* iKO SNs (Figure 1F). These results suggest that WT SCs express all four TEADs and
135 that *Tead1* cKO and iKO SCs express TEAD2-4 in their nuclei.
136
137 **YAP/TAZ strongly favor TEAD1 but partner with other TEADs in the absence of TEAD1**
138 In the absence of a partner TF, nuclear YAP/TAZ are decreased and phosphorylation of
139 YAP/TAZ increased, due to targeting by Large tumor suppressor kinase 1/2 (LATS1/2),
140 negative regulators of YAP/TAZ (Meng et al., 2016). To investigate if YAP/TAZ are in the
141 nuclei of SCs and therefore transcriptionally functional in the absence of TEAD1, we compared
142 western blotting of P50 WT vs *Tead1* cKO SN lysates and observed an overall decrease in YAP
143 levels in *Tead1* cKO but a > 2-fold increase in TAZ levels compared to WT (Figure 2A). This
144 ratio of YAP to TAZ in *Tead1* cKO resembled that observed during developmental myelination
145 in WT SNs (Deng et al., 2017; Grove et al., 2017). Furthermore, phosphorylation of YAP
146 decreased in cKO, which would typically indicate increased YAP activity. These results suggest

147 that YAP/TAZ are not targeted for destruction in the absence of TEAD1. Indeed, YAP/TAZ
148 were retained in the SC nucleus of *Tead1* cKO (Figure 2B) and both intact and injured *Tead1*
149 iKO SNs (Figure 2C, 2D), as strongly supported by quantitative analysis (Figure 2E).
150 To investigate whether other TEADs could be complexed with YAP/TAZ, thereby
151 retaining YAP/TAZ in SC nuclei in the absence of TEAD1, we carried out YAP/TAZ co-
152 immunoprecipitation (IP) experiments comparing WT vs *Tead1* iKO, and blotted for YAP/TAZ,
153 TEAD1 and pan-TEAD (Figure 2F). After verifying equal amounts of lysate samples and the
154 efficiency of IPs with post-IP lysates, we observed that TEAD1 strongly co-IPed with YAP/TAZ
155 from WT lysates and that levels were greatly reduced in *Tead1* iKO lysates. Blotting with anti-
156 pan-TEAD showed that multiple TEADs were co-IPed with YAP/TAZ from both WT and *Tead1*
157 iKO lysates. Notably, the pan-TEAD co-IPed from WT lysates, like TEAD1, migrated more
158 slowly than that from *Tead1* iKO lysates, whereas the *Tead1* iKO pan-TEAD migrated similarly
159 to the major pan-TEAD band in post-IP lysates. Longer exposure of the pan-TEAD film revealed
160 the presence of a fainter band migrating above the main pan-TEAD band in WT lysates (Figure
161 2F; arrow). Because this band co-migrated with TEAD1 and was not present in *Tead1* iKO
162 lysates, it was identified as TEAD1. These results suggest that TEAD1 makes up a very minor
163 portion of that revealed by pan-TEAD in WT lysates, but the overwhelming majority of that
164 revealed by pan-TEAD in YAP/TAZ IPs from these lysates. Therefore, although multiple
165 TEADs are present, TEAD1 is greatly favored as the binding partner for YAP/TAZ. However, in
166 the absence of TEAD1, other TEADs are associated with YAP/TAZ presumably to substitute for
167 some or all the functions of the YAP/TAZ-TEAD1 transcriptional complex.
168
169 **TEAD1 is required for myelin sheath formation and growth**
170 *Tead1* cKO mice were smaller than WT mice at all ages, with labored breathing and
171 severely splayed fore- and hindlimbs, indicative of severe peripheral neuropathy (Figure 3A,
172 Supplementary Video 1). The hindlimbs never became completely paralyzed, however, in
173 contrast to *Yap/Taz* cDKO mice (Grove et al., 2017). *Tead1* cKO mice were humanely
174 euthanized before P60. *Tead1* cKO SNs were noticeably translucent, indicative of reduced
175 myelin content (Figure 3B). Electrical stimulation of cKO SNs elicited low and dispersed
176 compound muscle action potentials (CMAPs) (Figure 3C). Nerve conduction velocity (NCV) in
177 cKO was ~8 m/s, which was markedly reduced from ~40 m/s in WT mice (Figure 3D).

178 Next, we used semi-thin and transmission electron microscopy (TEM) to examine the
179 processes of developmental myelination and Remak bundle formation. We first examined SNs at
180 P3, when, in WT, many large axons had already been radially sorted, establishing 1:1
181 relationship with promyelinating SCs, and myelination had begun. Compared to WT, *Tead1* cKO
182 SNs were thinner, unsorted bundles of axons were larger and more numerous, and myelination
183 was minimal (Figure 3E). Nevertheless, we frequently observed large axons that had been sorted
184 and established a 1:1 relationship with promyelinating SCs, as in WT. Therefore, radial sorting
185 was delayed in *Tead1* cKO, though less severely than in *Yap/Taz* cDKO mice, in which no axons
186 were sorted at P4 (Grove et al., 2017).
187 At P22, when WT SNs were fully myelinated, the phenotype of *Tead1* cKO SNs was
188 complex and included areas of unsorted axon bundles, sorted but unmyelinated axons, and thinly
189 myelinated axons (Figure 3F, Supplementary figure 1A). Notably, at P50, this phenotype was
190 unchanged from that at P22: areas of unsorted bundles, promyelination, and thin myelination
191 persisted (Figure 3G, Supplementary figure 1A). TEM analysis confirmed that myelin was
192 indeed thinner in *Tead1* cKO than in WT at both P22 and P50 (Figure 3F, 3G, Supplementary
193 figure 1B). The g-ratio did not significantly change in either WT or cKO between P22 and P50
194 (Figure 3H), suggesting that growth of the myelin sheath relative to axon diameter did not
195 increase over this period. These data suggest that myelination in *Tead1* cKO was arrested rather
196 than delayed. Plots of g-ratio versus axon diameter showed that the mutant defect was present in
197 axons of all diameters but was particularly notable in those of larger diameter (Figure 3I, 3J).
198 The mean axon diameter was also reduced in cKO at P22, though it increased with age (Figure
199 3K). These data show that TEAD1 is required, like YAP/TAZ (Grove et al., 2017), for timely
200 radial sorting and initiation of myelination during development. Although some axons become
201 myelinated in the absence of TEAD1, presumably due to other TEADs, they require TEAD1 for
202 myelin sheath to properly grow in proportion to axon diameter.
203
204 **TEAD1 is required for proper formation of Remak bundles**
205 Remak bundle formation was also abnormal in *Tead1* cKO mice. In WT SNs at P22 and
206 P50, small diameter axons were present in Remak bundles, with each C-fiber ensheathed by SC
207 cytoplasm (Figure 3F, 3L). In *Tead1* cKO, C-fibers were also present in bundles in which axons
208 were rarely larger than 1 μm in diameter, suggesting that they were almost fully sorted.

209 However, at both P22 and P50, the observed bundles were frequently small, often the size of a
210 large myelinated axon. Notably, a SC surrounded each bundle but individual C-fibers of most
211 Remak bundles were not ensheathed by SC cytoplasm (Figure 3L). Furthermore, these bundles
212 were frequently and abnormally thinly myelinated. Quantification showed that ~80% of C-fibers
213 were not ensheathed by SC cytoplasm in P50 *Tead1* cKO SNs (Figure 3M). Therefore, TEAD1
214 is required to develop proper association of C-fibers with non-myelinating SCs in Remak
215 bundles.
216
217 **TEAD1 regulates SC proliferation both positively and negatively to promote myelination**
218 For myelination and Remak bundle formation to occur properly, timely generation of
219 sufficient numbers of SCs is essential. YAP/TAZ are necessary for optimal SC proliferation in
220 the late embryonic and early postnatal periods (Deng et al., 2017; Feltri et al., 2016; Grove et al.,
221 2017). To determine if the defects of myelination and Remak bundles in *Tead1* cKO are due to
222 defective SC proliferation, we counted SCs. At P3, SC number in cKO SNs was about half that
223 of WT (Figure 4A), slightly more than in *Yap/Taz* cDKO at P4 (Grove et al., 2017). The number
224 of SCs in the cell cycle (Ki67-positive; Figure 4B) and in S-phase (EdU-positive; Figure 4C) was
225 greatly reduced in cKO at P3. Therefore, TEAD1 is required for optimal SC proliferation at P3,
226 suggesting that the YAP/TAZ-TEAD1 complex promotes SC proliferation at early postnatal
227 periods.
228 At P22 and P50, however, SC numbers in *Tead1* cKO SNs were greatly increased and
229 became more than twice those of WT (Figure 4A); a similar increase was not observed in
230 *Yap/Taz* cDKO (Grove et al., 2017). As *Tead1* cKO SC numbers were similar at P22 and P50,
231 we reasoned that between P3 and P22, SC proliferation must occur at an abnormally high rate in
232 this mutant. Indeed, the number of SCs that were Ki67-positive or EdU-positive was
233 significantly increased in cKO at P22 (Figure 4B, 4C). The increased SC numbers were not due
234 to proliferation of residual non-deleted SCs: whereas in WT, EdU-positive SCs contained
235 TEAD1, TEAD1 was absent in most EdU-positive SCs in *Tead1* cKO (Figure 4D). During
236 development, therefore, SCs switch from requiring TEAD1 for optimal proliferation, to requiring
237 TEAD1 for timely exit from the cell-cycle, which is a prerequisite for SC differentiation and
238 myelination (Hindley and Philpott, 2012).
239

240 **TEAD1 is required for Krox20 to upregulate myelin proteins, but not for Krox20**
241 **upregulation**
242 Our findings thus far show that, in the absence of TEAD1 in SCs, other TEADs can
243 complex with YAP/TAZ. Nevertheless, only some axons are myelinated abnormally thinly in
244 *Tead1* cKO which grossly phenocopied *Yap/Taz* iDKO. These defects are not because *Tead1*
245 cKO mice lack SCs. *Yap/Taz* cDKO exhibited a complete failure of myelination due to arrest of
246 their SCs as promyelinating SCs, in part because they fail to upregulate Krox20/Egr2 (Early
247 Growth Response 2), which drives transcription of myelin proteins (Grove et al., 2017). To
248 determine whether TEAD1 is required for Krox20 upregulation, we first investigated Oct6
249 (Pou3f1, Scip), whose upregulation precedes and is required for Krox20 upregulation; Oct6 is
250 subsequently downregulated, possibly by Krox20 in a feedback mechanism (Ryu et al., 2007;
251 Zorick et al., 1999). Western blotting of P50 SN lysates showed minimal expression of Oct6 in
252 WT, but greatly upregulated expression in *Tead1* cKO (Figure 5A). Immunohistochemistry of
253 P50 cKO SNs showed intense Oct6 expression in ~80% of SC nuclei; Oct6 expression was
254 minimal in WT (Figure 5B). Notably, at both P11 and P50, a similar percentage of SCs
255 expressed Krox20 in WT and *Tead1* cKO SNs (Figure 5C). In Western blots, Krox20 was
256 upregulated >4-fold in cKO compared to WT (Figure 5A). As adult *Tead1* cKO mice contain ~2-
257 fold more SCs than WT (Figure 4A), these data suggest that each SC in *Tead1* cKO contains ~2-
258 fold more Krox20 than WT. Thus, in contrast to SCs lacking YAP/TAZ (Grove et al., 2017), SCs
259 lacking TEAD1 upregulate Krox20, suggesting that TEAD1 is dispensable for YAP/TAZ to
260 upregulate Krox20.
261 Consistent with the idea that Krox20 is pivotal for myelin gene transcription, expression
262 of myelin basic protein, MBP, and myelin protein zero, MPZ, was abundant in WT P50 SNs
263 (Figure 5A). In contrast, despite ample expression of Krox20, both MBP and MPZ were
264 markedly decreased in *Tead1* cKO, suggesting that Krox20 fails to properly upregulate myelin
265 proteins without TEAD1. To exclude the possibility that Krox20 expressed in cKO SCs is
266 defective, we took advantage of the earlier finding that loss of Krox20 or its co-factors, Nab1/2,
267 causes SCs to remain aberrantly in the cell-cycle (Le et al., 2005b; Zorick et al., 1999).
268 Therefore, we studied whether EdU-positive SCs in the cell-cycle of P11 cKO were also positive
269 for Krox20, which would indicate defective Krox20. We found that, although ~65% of SC nuclei
270 contained Krox20, only a few EdU-positive SCs exhibited even minimal Krox20

271 immunoreactivity in either WT or *Tead1* cKO (Figure 5D). Thus, despite high levels of
272 functional Krox20, myelin protein expression was greatly reduced in cKO SCs, suggesting that
273 TEAD1 is dispensable for Krox20 upregulation but required for Krox20 to upregulate myelin
274 proteins.
275
276 **TEAD1 and YAP/TAZ upregulate cholesterol biosynthetic enzymes, FDPS and IDI1**
277 Myelination of peripheral nerves by SCs requires a large amount of lipid and cholesterol
278 biosynthesis. De novo biosynthesis of fatty acids (integral building blocks of lipids) and
279 cholesterol is crucially important for SCs to initiate myelination and to grow a myelin sheath
280 (Montani et al., 2018; Norrmen et al., 2014; Saher et al., 2009; Verheijen et al., 2009). YAP/TAZ
281 may regulate these pathways, as suggested by reduced mRNA expression in *Yap/Taz* cDKO of
282 SREBPs TFs (Sterol regulatory element binding proteins) and their target enzymes involved in
283 lipid/cholesterol biosynthesis (Deng et al., 2017; Poitelon et al., 2016). We therefore
284 investigated, at the protein level, whether TEAD1 and YAP/TAZ are required for fatty acid
285 and/or cholesterol synthesis. To test this premise, we examined expression of SREBP1 and its
286 target SCD1 (Stearoyl-CoA desaturase-1), which upregulates fatty acid synthesis, and of
287 SREBP2 and its targets HMGCR (HMG-CoA reductase), FDPS (Farnesyl Diphosphate
288 Synthase) and IDI1 (Isopentenyl-diphosphate delta isomerase 1), which upregulate cholesterol
289 synthesis (Leblanc et al., 2005; Verheijen et al., 2009). Because SREBP pathways are
290 upregulated early postnatally for myelination in WT SNs, their upregulation may simply be
291 delayed in developmentally delayed *Tead1* cKO. We therefore investigated SREBP pathways
292 both at P8 and P40 in WT and *Tead1* cKO mice. Western blot analysis showed that levels of
293 nuclear SREBP1 was not affected by loss of TEAD1 at P8, and only slightly reduced at P40
294 (Figure 6A). SCD1 was reduced at P8, but slightly increased at P40. In contrast to SREBP1,
295 SREBP2 was ~50% reduced in *Tead1* cKO at both P8 and P40. Despite marked reduction in
296 SREBP2, HMGCR was not reduced at P8 or P40. However, both FDPS and IDI1 levels were
297 greatly reduced at both P8 and P40 (Figure 6A).
298 It is possible that HMGCR was not reduced in cKO due to TEAD1 redundancy and
299 compensation by other TEADs. If so, then HMGCR levels should be reduced in *Yap/Taz* cDKO,
300 because YAP/TAZ are the primary partners for all TEADs (Holden and Cunningham, 2018;
301 Zheng and Pan, 2019). To test this idea, we examined SREBP pathways in *Yap/Taz* cDKO SNs

302 at P60 because developmental delay is greater in *Yap/Taz* cDKO than in *Tead1* cKO SNs (Grove
303 et al., 2017). We found that, as in *Tead1* cKO, SREBP1 levels were unaffected and SCD1 levels
304 were markedly increased by the loss of YAP/TAZ in cDKO at P60 (Figure 6B). Unlike in *Tead1*
305 cKO, levels of SREBP2 were not markedly reduced in Yap/Taz cDKO. As in *Tead1* cKO,
306 however, HMGCR levels were not reduced in Yap/Taz cDKO, whereas levels of FDPS and IDI1
307 were greatly reduced (Figure 6B). These results therefore suggest that YAP/TAZ-TEAD1
308 transcriptional complex selectively upregulates IDI1 and FDPS, contributing to cholesterol
309 biosynthesis. Together with the lack of synthesis of myelin proteins, this reduction in cholesterol
310 biosynthesis may prevent myelin formation and growth in *Tead1* cKO.
311
312 **Loss of TEAD1 in adult Schwann cells modestly affects myelin maintenance**
313 Because TEAD1 regulates myelination and Remak bundle formation during
314 development, we next investigated its role in myelin and Remak bundle maintenance in adults.
315 We first verified efficient deletion of TEAD1 in almost all SCs of *Tead1* iKO (Figure 1B).
316 Unlike *Yap/Taz* iDKO mice (Grove et al., 2017), *Tead1* iKO mice appeared normal 2 weeks after
317 tamoxifen administration and continued to survive without obvious signs of peripheral
318 neuropathy up to 5 months post-tamoxifen, the longest time of observation (Figure 7A). Analysis
319 of iKO SNs between 3 to 5 months post-tamoxifen revealed that they were grossly normal.
320 However, we occasionally observed large axons undergoing demyelination or completely
321 demyelinated (Figure 7B). Unlike *Yap/Taz* iDKO mice, which frequently exhibited segmental
322 demyelination and markedly reduced NCV (Grove et al., 2017), NCV of these iKO mice did not
323 significantly differ from that of WT (Figure 7C). Therefore, loss of TEAD1 alone in adult SCs
324 evoked only modest demyelination that does not cause significant functional impairment.
325
326 **TEAD1 is required for maintaining structural integrity of Remak bundles**
327 Next, we examined Remak bundles in these mice. As in WT SNs, C-fibers in WT mice
328 were individually ensheathed by SC cytoplasm. In contrast, in *Tead1* iKO, many c-fibers in most
329 Remak bundles were not separated by SC cytoplasm (Figure 7D). Furthermore, some Remak
330 bundles were abnormally myelinated, as in *Tead1* cKO SNs (Figure 7E). Thus, TEAD1 is
331 required for formation as well as maintenance of Remak bundles.
332

333 **TEAD1 is dispensable for YAP/TAZ to maintain Krox20, FDP and IDI1 expression**

334 To investigate why the demyelinating phenotype of *Tead1* iKO is much milder than that
335 of *Yap/Taz* iDKO, we first investigated expression of Krox20 which is required for myelin
336 maintenance (Decker et al., 2006). We previously observed that Krox20 is markedly
337 downregulated in *Yap/Taz* iDKO SCs, which correlated with frequent segmental demyelination
338 and markedly reduced NCV (Grove et al., 2017). As a control, we injected *PLP-CreER; Yap*$^{fl/fl}$*;*
339 *Taz*$^{fl/fl}$ mice with tamoxifen and reproduced our previous result: Krox20 was dramatically
340 downregulated in most *Yap/Taz* iDKO SCs only 2 weeks post-tamoxifen (Figure 7F). In contrast,
341 in *Tead1* iKO, Krox20 expression was indistinguishable from WT even at 6 weeks post-
342 tamoxifen (Figure 7G). We then investigated Oct6 expression, because aberrant overexpression
343 of Oct6 in the presence of Krox20 inhibits myelination (Ryu et al., 2007). Unlike in *Yap/Taz*
344 iDKO SNs (Grove et al., 2017), however, Oct6 was not elevated in *Tead1* iKO SNs (Figure 7H).
345 Therefore, TEAD1 is dispensable for maintaining Krox20 expression in myelinating SCs,
346 consistent with the only modest demyelinating phenotype of *Tead1* iKO.

347 Next, we investigated SREBP pathways, which are required for developmental
348 myelination (Saher et al., 2009; Verheijen et al., 2009). Whether these pathways are also
349 involved in myelin maintenance has not been studied. We first assessed the effects of acute loss
350 of YAP/TAZ on these pathways in adult SCs. Western blotting of WT and *Yap/Taz* iDKO SN
351 lysates showed that the SREBP1 pathway, or expression of SREBP2 and HMGCR in the
352 SREBP2 pathway, was unaffected in *Yap/Taz* iDKO (Figure 7I). However, FDPS and IDI1
353 levels were significantly downregulated in *Yap/Taz* iDKO (Figure 7I), recapitulating the effect of
354 developmental loss of YAP/TAZ on these proteins (Figure 6B). Therefore, the acute
355 downregulation of these key enzymes for cholesterol biosynthesis correlates with the acute
356 demyelination previously observed in *Yap/Taz* iDKO mice. This result suggests that YAP/TAZ
357 maintain myelination through both myelin gene expression and the cholesterol biosynthesis
358 pathway.

359 Western blotting of *Tead1* iKO SN lysates, 6 weeks post-tamoxifen, revealed that the
360 SREBP pathways were not significantly affected by loss of TEAD1 (Figure 7J), unlike *Tead1*
361 cKO in which FDPS and IDI1 were markedly downregulated. This result correlated with the
362 modest effect of loss of TEAD1 on myelin maintenance, suggesting that TEAD1 is largely
363 dispensable for cholesterol synthesis in adult SCs.

364

365 **TEAD1 is required for myelination of regenerating axons after nerve injury**.

366 Next, we investigated whether TEAD1 is required for axon regeneration and
367 remyelination after nerve injury. We previously showed that YAP/TAZ are not required for axon
368 regeneration but are necessary for remyelination (Grove et al., 2017). Because *Yap/Taz* iDKO
369 mice die ~2 weeks post-injury, it remains possible that remyelination is delayed rather than
370 completely blocked. In contrast, *Tead1* iKO mice are not susceptible to early death. We,
371 therefore, examined them 4 weeks after crushing SN, when hindlimb muscles are fully
372 reinnervated in WT (Figure 8A). We first verified efficient deletion of TEAD1 in almost all SCs
373 of *Tead1* iKO mice after nerve crush (Figure 1C). Longitudinal sections of iKO SNs showed
374 numerous TuJ1-labeled axons that regenerated along the distal nerve stump, as in WT SNs
375 (Figure 8B). However, MBP immunoreactivity was markedly reduced in the distal nerve stump
376 of *Tead1* iKO, compared to WT, suggesting that axons regenerated but were not remyelinated.
377 We also found that regenerated axons reached hindlimb muscles and reinnervated neuromuscular
378 junctions (NMJs) in iKO, as in WT (Figure 8C). Moreover, *Tead1* iKO frequently exhibited
379 features of paralyzed muscles, such as axon terminals that grew past the synaptic area,
380 fragmented clusters of acetylcholine receptors (AChRs), and satellite extra-synaptic AChRs
381 (Wright et al., 2007). Semithin and EM analysis confirmed virtual absence of myelination in iKO
382 SNs; although large axons were associated with SCs, they were not myelinated (Figure 8D).
383 Accordingly, electrical stimulation of iKO SNs did not elicit CMAPs or NCV (Figure 8E). Thus,
384 like YAP/TAZ, TEAD1 in SCs is not required for axon regeneration but is required for
385 remyelination after nerve injury.

386 After injury, SCs transdifferentiate into growth-promoting repair SCs, which then
387 proliferate and reach a peak around 3 dpi (Clemence et al., 1989; Jessen and Mirsky, 2016;
388 Tricaud and Park, 2017). Quantitative analysis of SC proliferation at 3 dpi by counting
389 $EdU^+/Sox10^+$ SCs showed that a similar percentage of SCs were in S-phase in both WT and
390 *Tead1* iKO SNs (Figure 8F), suggesting that, like YAP/TAZ (Grove et al., 2017), TEAD1 is not
391 required for proliferation of repair SCs. Lastly, we counted $Krox20^+$ and $Oct6^+$ SCs at 4 wpi.
392 Notably, in contrast to *Yap/Taz* iDKO SCs, which fail to upregulate Krox20 after injury (Grove
393 et al., 2017), Krox20 was upregulated in *Tead1* iKO SCs, as in WT SCs (Figure 8G).
394 Furthermore, Oct6 was aberrantly elevated in *Tead1* iKO SCs, like in *Tead1* cKO SCs during

395 development (Figure 8H). These results suggest that, similar to developmental myelination,
396 remyelination requires TEAD1 for Oct6 downregulation and for Krox20 to upregulate myelin
397 proteins. Additionally, almost complete absence of remyelination at 4 wpi highlights that
398 TEAD1 is crucial for functional regeneration of peripheral nerves.
399
400 **DISCUSSION**
401 The present study conclusively establishes TEAD1 as a crucial TF that partners with YAP/TAZ
402 to mediate myelin formation, growth, and regeneration. TEAD1 promotes myelination by dually
403 regulating SC proliferation, by enabling induced Krox20 to upregulate myelin proteins, and by
404 upregulating cholesterol biosynthetic enzymes. Our findings also suggest that other TEADs play
405 redundant and opposing roles in SCs, and that TEAD1 is critical in the proper formation and
406 maintenance of Remak bundles.
407
408 **Unique, redundant, and opposing roles of TEAD1**
409 Although SCs express all four TEADs, *Tead1* cKO mice grossly phenocopies *Yap/Taz* cDKO
410 mice. They exhibit abnormal SC proliferation, delayed radial sorting, blocked myelin formation
411 and remyelination, and normal axon regeneration. Furthermore, *Tead1* cKO mice, like *Yap/Taz*
412 cDKO, are defective in regulating Oct6, Krox20, myelin proteins, and enzymes that synthesize
413 cholesterol. These similarities show that YAP/TAZ regulate both SC proliferation and
414 differentiation, the two opposing processes crucial for myelination, by partnering mainly with
415 TEAD1 at least for developmental myelination and remyelination after injury.
416
417 We also observed multiple differences between *Tead1* cKO and *Yap/Taz* cDKO mutants. Unlike
418 *Yap/Taz* cDKO, *Tead1* cKO initiates myelin formation in some developing axons and maintain
419 myelination in most axons but fails to remyelinate almost all regenerating axons. Additionally, in
420 *Tead1* cKO, Krox20 are upregulated and a large excess of SCs is generated. These differences
421 are likely due to stage-dependent redundancy and opposing roles of TEADs. Consistent with this
422 idea, YAP/TAZ functionally associate with TEAD2, 3 or 4, or an unrelated TF (Varelas, 2014),
423 in the absence of TEAD1. Loss of TEAD1 does not affect nuclear localization of YAP/TAZ,
424 which depends mainly on interactions with TEADs (Diepenbruck et al., 2014; Kim et al., 2020;
425 Kofler et al., 2018; Yao et al., 2018). Our data and the results of others suggest that TEAD1-4

426 are all co-expressed in SCs through multiple stages of nerve development, homeostasis and after
427 injury (Fernando et al., 2016; Grove et al., 2017; He et al., 2018). Notably, nuclear retention of
428 YAP/TAZ occurs in *Tead1* cKO when TEAD1 has a unique role in SCs (i.e., when *Tead1* cKO
429 SCs fail to form and re-form myelination). Therefore, other TEADs can retain nuclear
430 YAP/TAZ, thereby supporting transcriptional activity of YAP/TAZ, but cannot substitute for
431 some or most of its functions with TEAD1 in a stage-dependent manner.
432
433 It is also notable that, like YAP/TAZ, the unique roles of TEAD1 change dynamically in
434 successive steps of myelination, even though other TEADs are present. Thus, TEAD1 is
435 uniquely required for timely proliferation of SCs during radial sorting; uniquely opposes SC
436 proliferation to promote cell-cycle exit after radial sorting; redundantly promotes upregulation of
437 Krox20; and then uniquely promotes upregulation of myelin proteins and cholesterol
438 biosynthetic enzymes. Such unique and redundant roles for TEAD1 in the presence of other
439 TEADs are supported by cell-based transcription assays, in which YAP-TEAD4 can substitute
440 for YAP-TEAD1 in upregulating transcription from the Krox20 promoter, but not from the MPZ
441 intronic enhancer (Fernando et al., 2016). Our data also show that even when TEAD1 is largely
442 redundant because other TEADs are present and can functionally substitute for TEAD1, such as
443 in myelin maintenance, YAP/TAZ preferentially bind to TEAD1. This situation resembles the
444 dynamic function of TEADs in cortical development, another multi-step differentiation program.
445 As in nerve development, multiple TEADs (TEAD1-3) are co-expressed throughout cortical
446 development. Depending on the differentiation stage, TEAD1 uniquely promotes proliferation,
447 redundantly promotes proliferation with TEAD2 and 3, or redundantly promotes differentiation
448 with TEAD3, when it is opposed by TEAD2 (Mukhtar et al., 2020).
449
450 As *Yap/Taz* cDKO SCs arrest at the promyelination stage, we were unable to investigate the role
451 of YAP/TAZ in myelin sheath growth (Grove et al., 2017). In contrast, some *Tead1* cKO SCs
452 can myelinate but fail to grow myelin sheaths proportional in size to axon diameter. Importantly,
453 such myelinating SCs apparently lack TEAD1 because TEAD1 deletion is extremely efficient in
454 *Tead1* cKO mice. Support for a role of TEADs in the regulation of myelin sheath thickness
455 comes from a study of TEAD4 cKO mice, in which SCs lacking TEAD4 gradually upregulate
456 myelin protein expression, resulting in adult mice with abnormally thick myelin (He et al., 2018).

457 Therefore, TEADs 1 and 4 oppose each other in the regulation of myelin sheath growth.
458 Likewise, they may oppose each other in the regulation of SC proliferation, resulting in a large
459 excess of SCs we observed in P22 and P50 *Tead1* cKO.
460
461 **TEAD1 regulation of Krox20 and myelin gene expression**
462 Previous work suggests that YAP/TAZ-TEAD1 promote myelination in part through direct
463 upregulation of Krox20 (Deng et al., 2017; Grove et al., 2017). Unlike *Yap/Taz* cKO mice,
464 *Tead1* cKO mice upregulate Egr2/Krox20, but they fail to upregulate myelin proteins and
465 cholesterol biosynthetic enzymes. Our findings extend previous work to suggest that TEAD1
466 functions redundantly in direct upregulation of Krox20, but that its function is required for
467 upregulated Krox20 to promote myelination. Krox20 activity may be repressed in *Tead1* cKO by
468 Oct6, which remains abnormally elevated. In support of this possibility, persistently elevated
469 Oct6 overrides Krox20 to inhibit myelin gene expression (Monuki et al., 1993; Ryu et al., 2007).
470 Other mice with defective lipid biosynthesis and a phenotype like *Tead1* cKO also have
471 abnormally elevated Oct6 after Krox20 upregulation (Norrmen et al., 2014; Sherman et al.,
472 2012). An alternative or additional possibility is that a transcriptional co-activator that synergizes
473 with Krox20 is absent in *Tead1* cKO SCs. We suggest that TEAD1 itself may function as such a
474 factor. Supporting this idea are reports that gene regulatory elements function by co-binding
475 several TFs, which synergistically activate transcription (Heinz et al., 2015; Ren and Yue, 2015),
476 as at the Krox20 MSE (Myelinating Schwann cell element) which is the enhancer responsible for
477 Krox20 expression (Ghislain and Charnay, 2006; Grove et al., 2017; He et al., 2010; Kao et al.,
478 2009). Krox20 synergizes with Sox10 to activate myelin genes (Jones et al., 2007) and with
479 SREBP to activate lipid biosynthesis genes (Leblanc et al., 2005). Like Krox20, TEAD1 can
480 directly promote transcription from PMP22 and MPZ myelin gene enhancers (Fernando et al.,
481 2016; Lopez-Anido et al., 2016). A consistent finding of the present work is that functional
482 Krox20 is insufficient to drive myelin/cholesterol gene expression in the absence of TEAD1.
483 Alternatively, or additionally, TEAD1 may also function indirectly by upregulating co-factors,
484 such as SREBP2, which is reduced in *Tead1* cKO. Notably, lipid biosynthesis is necessary to
485 downregulate Oct6 and upregulate myelin gene transcription during developmental myelination
486 (Saher et al., 2009; Verheijen et al., 2009). An interesting possibility, therefore, is that

487 YAP/TAZ-TEAD1 and Krox20 may cooperatively downregulate Oct6 and upregulate myelin
488 gene expression at least in part by promoting lipid biosynthesis.
489
490 **YAP/TAZ-TEAD1 regulation of cholesterol biosynthesis**
491 SREBP1 levels are not altered in *Tead1* cKO or *Yap/Taz* cDKO, suggesting that fatty acid
492 synthesis is not directly regulated by YAP/TAZ or TEAD1. It is likely that the reduced levels of
493 SCD1 at P8 and slight increase at P40 in *Tead1* cKO, and the large increase in SCD1 in *Yap/Taz*
494 cDKO at P60 are due to developmental delay in these mutants. We did not observe
495 downregulation of HMGCR in *Tead1* cKO or *Yap/Taz* cDKO mice at P8 or P40, which
496 contradicts the report of reduced mRNA expression of HMGCR in *Yap/Taz* mutants at P3 and P5
497 (Deng et al., 2017; Poitelon et al., 2016); we suggest this difference is due to developmental
498 delay in *Tead1* cKO and *Yap/Taz* cDKO. However, marked downregulation of IDI1 and FDPS in
499 *Tead1* cKO, *Yap/Taz* cDKO, and *Yap/Taz* iDKO suggests that cholesterol biosynthesis is
500 defective in these mutants. In support of this notion, SC-selective deletion of SCAP (SREBP
501 cleavage activation protein), which is required to produce active SREBP1 and SREBP2
502 (Verheijen et al., 2009), or of Squalene synthase, an essential enzyme in cholesterol biosynthesis
503 (Saher et al., 2009), evokes phenotypes which are remarkably similar to those of *Tead1* cKO
504 mice: both mutants have an increased number of SCs, a severe delay at the promyelination stage,
505 and persistently thin myelin. In addition, in SCAP cKO, Oct6 is upregulated continuously and
506 Squalene synthase cKO fails to upregulate myelin gene transcription, resulting in severely
507 reduced MBP, MPZ, and PMP22 protein levels.
508
509 How might YAP/TAZ-TEAD1 regulate IDI1 and FDPS? Multiple studies show that YAP/TAZ
510 can activate the mTORC1 pathway (Hu et al., 2017; Kim et al., 2015), and IDI1 and FDPS levels
511 are reduced in Raptor cKO SNs (Norrmen et al., 2014). Furthermore, the Raptor cKO phenotype
512 is like that of *Tead1* cKO, exhibiting an increased number of SCs, normal upregulation of
513 Krox20, persistent upregulation of Oct6, delay at the promyelination stage, and thin myelin.
514 However, HMGCR protein levels are reduced, and aberrant upregulation of Oct6 is transient
515 (Norrmen et al., 2014). Furthermore, after nerve injury, formation of repair SCs is delayed in
516 Raptor mutants (Norrmén et al., 2018), unlike TEAD1 and YAP/TAZ mutants. These differences
517 suggest that YAP/TAZ-TEAD1 are not directly upstream of mTORC1. Another possibility is

518 that YAP/TAZ-TEAD1 may directly regulate transcription of IDI1 and FDPS genes. Such direct
519 regulation of cholesterol biosynthetic enzymes has been observed for other TFs in SCs (Kim et
520 al., 2018; Leblanc et al., 2005).
521
522 **TEAD1 regulation of Remak bundles**
523 In both *Tead1* cKO and iKO mice, there is defective ensheathment of C-fibers by SCs in Remak
524 bundles, which are occasionally thinly myelinated. This phenotype is distinct from those mutants
525 in which SCs surround and sometimes myelinate bundles filled with mixed-caliber axons, which
526 are considered radial sorting defects (Feltri et al., 2016). Remak bundles can myelinate
527 abnormally in WT SNs during early postnatal development, but this defect is corrected and does
528 not persist in adults (Rasi et al., 2010). Therefore, the defective Remak bundles that we observed
529 in *Tead1* cKO are not due to developmental delay, and the defects found in adult *Tead1* iKO
530 appear unusual.
531
532 Remak bundles form normally at P60 in *Yap/Taz* cDKO, although many large bundles containing
533 mixed caliber axons are present during development (Grove et al., 2017). The difference between
534 *Tead1* and *Yap/Taz* mutants is supported by the presence of TEAD1 and absence of YAP/TAZ in
535 non-myelinating SC nuclei (Grove et al., 2017). Notably, defective SC ensheathment of C-fibers
536 and myelinated Remak bundles is observed in various SC developmental mutants, including
537 those with defective SC basal lamina (Rasi et al., 2010) and overexpression of NRG1-IIIb in
538 axons (Gomez-Sanchez et al., 2009). Therefore, it is possible that TEAD1 mediates extracellular
539 signaling from the SC basal lamina and/or axons that is responsible for forming and maintaining
540 proper association of SCs with C-fibers. Notably, SC ensheathment of C-fibers is required for
541 normal NCV (Taveggia et al., 2005), and NCV with tg-NRG1-IIIb Remak bundles is reduced
542 compared to WT (Gomez-Sanchez et al., 2009). Future studies will address NRG1 signaling and
543 NCV in cKO and iKO mice lacking TEAD1 and/or other TEADs.
544
545 **MATERIALS AND METHODS**
546
547 **Animals**

548 All surgical procedures and animal maintenance complied with the National Institute of Health
549 guidelines regarding the care and use of experimental animals and were approved by the
550 Institutional Animal Care and Use Committee of Temple University, Philadelphia, PA, USA.
551 Generation and genotyping of mice carrying targeted loxP sites in the *Tead1* gene have been
552 described previously (Wen et al., 2017). Targeted ablation of *Tead1* in Schwann cells of
553 embryonic mice was achieved by crossing *Tead1*$^{fl/fl}$ mice with mice transgenic for *Cre* driven by
554 the *Mpz* promoter (*Tead1* cKO mice). Targeted ablation of *Tead1* in Schwann cells of adult mice
555 was by crossing *Tead1*$^{fl/fl}$ mice with mice transgenic for the inducible Cre recombinase *Cre-*
556 *ERT2* under control of the *Plp1* promoter (*Tead1* iKO mice). Control mice contained floxed
557 *Tead1* alleles but were not transgenic for *Cre* or *Cre-ERT2*. *Mpz-cre*;*Yap*$^{fl/fl}$; *Taz*$^{fl/fl}$ (*Yap/Taz*
558 cDKO) and *Plp1-creERT2*; *Yap*$^{fl/fl}$; *Taz*$^{fl/fl}$ (*Yap/Taz* iDKO) mice used in this study were
559 generated and genotyped as described previously (Grove et al., 2017). Both male and female
560 mice were used in all experiments and were maintained on the C57BL/6 background.
561
562 **Tamoxifen administration**
563 Tamoxifen was prepared and injected into 6–8-week-old *Tead1* or *Yap/Taz* mutant mice as
564 previously described (Grove et al., 2017). A 10 mg/ml solution of tamoxifen was made in 10:1
565 sunflower oil: 100% ethanol. This solution was injected intraperoneally at a concentration of 0.2
566 mg/g body weight. Injection was once daily for 5 days, followed by a 2-day break, then once
567 daily for 5 consecutive days.
568
569 **Nerve crush**
570 Sciatic nerves of right hindlimbs were crushed 24 h after the final tamoxifen injection, as
571 described previously (Grove et al., 2020; Son and Thompson, 1995). A small skin incision was
572 made in the posterior thigh and calf of the animals anesthetized by isoflurane. The sciatic nerve
573 was crushed with a fine forceps (#5) for 10 seconds (3X) adjacent to the sciatic notch. The crush
574 site was marked using charcoal-coated forceps, and the wound was closed. To identify
575 proliferating Schwann cells, we intraperitoneally injected EdU (80 μg/g) eighty minutes before
576 euthanasia, as previously described (Grove et al., 2017).
577
578 **Western blotting and immunoprecipitation**

579 After removal of epineurium and perineurium, sciatic nerves were snap-frozen in liquid nitrogen
580 and stored at -80ºC. For Western blotting, sciatic nerves were lysed in RIPA buffer (25 mM Tris
581 pH 7.5, 150 mM NaCl, 1% Triton X-100, 0.5% sodium deoxycholate, 1 mM EDTA, 0.1% SDS);
582 for immunoprecipitation, lysis was in co-IP buffer (50 mM Tris pH 8.0, 150 mM NaCl, 0.5%
583 Triton X-100, 10% glycerol, 1 mM EDTA), both containing protease and phosphatase inhibitors.
584 Lysis was for 40 minutes on ice, followed by microcentrifugation at 14,000 rpm for 20 minutes.
585 Protein concentration was determined using the BCA assay (ThermoFisher).
586 Immunoprecipitation was overnight at 4ºC, followed by 1 hour with protein A sepharose
587 (pre-blocked with 1% BSA), both with constant rotation. Lysates and immunoprecipitated
588 complexes in 1x Laemmli buffer were resolved on 8 or 10% SDS-PAGE gels, transferred to
589 nitrocellulose, and blotted with the appropriate antibodies. Primary antibodies were used at the
590 following concentrations for Western blots or immunoprecipitations: rabbit anti-Krox20
591 (Covance; 1:400), rabbit anti-Oct6 (Abcam ab126746; 1:1000), mouse anti-Myelin Basic Protein
592 (Covance SMI94; 1:1000), mouse anti-beta actin (SIGMA-Aldrich A5441; 1:5000), rabbit anti-
593 TEAD1 (Cell Signaling D9X2L, #12292; 1:1000), rabbit anti-TEAD2 (Novus Biologicals,
594 #NBP3-05267; 1:1000), rabbit anti-TEAD3 (Cell Signaling #13224; 1:1000), rabbit anti-TEAD4
595 (Santa Cruz, #sc-101184; 1:1000), rabbit anti-pan-TEAD (Cell Signaling, #13295; 1:1000),
596 rabbit anti-YAP/TAZ (Cell Signaling D24E4, #8418; 1:1000, 1:100 for immunoprecipitations),
597 rabbit anti-phospho-YAP(Ser127) (Cell Signaling D9W2I #13008; 1:1000), rabbit anti-phospho-
598 YAP(Ser397) (Cell Signaling D1E7Y #13619; 1:1000), rabbit-anti-MPZ (Cell Signaling #57518;
599 1:1000), mouse anti-SREBP1 (Novus Biologicals, #NB600-582; 1:1000), rabbit anti-SCD1 (Cell
600 Signaling, #2794; 1:1000), rabbit anti-SREBP2 (Bethyl laboratories, #A303-125A), rabbit anti-
601 HMGCR (Novus Biologicals, #NBP2-66888; 1:1000), rabbit anti-FDPS (Proteintech, #16129-1-
602 AP; 1:1000), rabbit anti-IDI1 (Proteintech, #11166-2-AP; 1:1000). Control whole rabbit IgG for
603 immunoprecipitations was from Jackson Laboratories (011-000-003) and was used at 1μg/ml,
604 which was several-fold greater than all other antibodies used for immunoprecipitations.
605 Secondary antibodies for Western blotting were HRP-linked sheep anti-mouse IgG and donkey
606 anti-rabbit (both GE Healthcare; 1:5000) and HRP-linked mouse anti-rabbit, light-chain specific
607 (Jackson ImmunoResearch 211-032-171; 1:20,000). Blots were developed using ECL, ECL Plus
608 (GE Healthcare) or Odyssey (LiCor).
609

610 **Immunohistochemistry, confocal and widefield fluorescence microscopy**

611 For immunostaining, sciatic nerves were removed and immediately fixed in 4%
612 paraformaldehyde in PBS for 1 hr. on ice. Nerves were washed 3 times in PBS, then stored in
613 15% sucrose in PBS overnight at 4°C for cryoprotection. Nerves were frozen-embedded in
614 cryoprotectant medium (Thermo Fisher Scientific, Waltham, MA) in isomethylbutane at -80°C.
615 7-10 μm sections from the nerves were cut using a cryostat (Leica Microsystems, Germany) and
616 collected directly onto glass slides. For immunolabeling, nerve sections were rehydrated in PBS,
617 permeabilized in 0.5% Triton/PBS for 20 min, washed with PBS, then blocked in 2% bovine
618 serum albumin (BSA) in PBS for 1 hr. Sections were incubated with primary antibodies in
619 blocking buffer overnight at 4°C in a hydrated chamber, washed with PBS, and incubated with
620 secondary antibodies in blocking buffer for 2 hrs. at room temperature. Sections were washed
621 with PBS, stained with DAPI for 10 min, and mounted with Vectashield mounting medium
622 (Vector Labs, Burlingame, CA).

623 Primary antibodies were used at the following concentrations for immunostaining of
624 cryosections: guinea pig anti-Sox10 (kind gift from Michael Wegner, University of Erlangen,
625 Bavaria, Germany; 1:1000), rabbit anti-Krox20 (Covance; 1:400), rabbit anti-Oct6 (Abcam
626 ab31766; 1:800), rabbit anti-Ki67 (Novocastra NCL-Ki67p; 1:200), rabbit anti-Neurofilament
627 200 (SIGMA-Aldrich N4142; 1:500), mouse anti-Neurofilament (Covance SMI 312; 1:1000),
628 mouse anti-Tubulin β3 (clone Tuj1, Covance #MMS-435P; 1:1000), mouse anti-SV2
629 (Developmental Studies Hybridoma Bank, Iowa; 1:10), rabbit anti-S100 (DAKO; 1:600), mouse
630 anti-Myelin Basic Protein (Covance SMI 94; 1:2000), rabbit anti-TEAD1 (Cell Signaling
631 D9X2L, #12292; 1:200), rabbit anti-pan-TEAD (Cell Signaling D3F7L, #13295; 1:200), rabbit
632 anti-YAP/TAZ (Cell Signaling D24E4, #8418; 1:200).

633 For immunostaining of extensor digitorum longus (EDL) and soleus muscles, mice were
634 perfused with 4% paraformaldehyde, and the muscles removed and post-fixed for 20 mins at
635 room temperature. Muscles were then incubated for 15 minutes with rhodamine-conjugated α-
636 bungarotoxin (Invitrogen, Carlsbad, CA), permeabilized in –20°C methanol for 5 min, and
637 blocked for 1 hr. in PBS containing 0.2% Triton and 2% BSA. The muscles were subsequently
638 incubated overnight at 4ºC in a cocktail of primary antibodies diluted in the blocking solution.
639 Axons and nerve terminals were labeled with mouse monoclonal antibodies to neurofilaments
640 (SMI 312; Sternberger Monoclonals, Baltimore, MD) and to a synaptic vesicle protein, SV2

641 (Developmental Studies Hybridoma Bank, Iowa City, IA). Schwann cells were labeled with
642 rabbit anti-cow S-100 polyclonal antibody (Dako, Carpentaria, CA). After incubation with the
643 primary antibodies, muscles were rinsed in PBS and incubated with secondary antibodies in the
644 blocking solution, for 1 hr. at room temperature. The muscles were then rinsed in PBS and
645 prepped for whole-mount by peeling the top layer of muscle fibers using microscissors and
646 forceps, as previously described (Son and Thompson, 1995). The resulting "muscle fillets" were
647 mounted on a slide and coverslipped.
648 Conventional fluorescence microscopy was performed using Olympus BX53 and Zeiss
649 Axio Imager 2 microscopes. Images were captured using Hamamatsu ORCA R2 C10600 or
650 Zeiss Axiocam HRm Rev 3 digital cameras, respectively, and Metamorph software. For confocal
651 microscopy, we used a Leica SP8 confocal microscope, with either a 40x 1.3 NA or 63x 1.4 NA
652 objective and Leica proprietary software. Acquired stacks were assembled using the maximum
653 projection tool, and figures were prepared using Adobe Photoshop.
654
655 **Electron microscopy, histology, and morphometry**
656 Mice were perfused intravascularly with 2.5% glutaraldehyde and 4% paraformaldehyde in 0.1M
657 cacodylate buffer pH 7.4. Sciatic nerves were removed and incubated in the same buffer for 90
658 minutes at room temperature, then overnight at 4°C. Specimens were post-fixed for 1 hr. with
659 OsO_4, dehydrated, then embedded in araldite. Semi-thin (0.5 μm) and ultrathin (70 nm) sections
660 were cut using an ultramicrotome and stained with toluidine blue or uranyl acetate and lead
661 citrate, respectively. Semi-thin sections were examined using bright field on an Olympus BX53
662 microscope, and images were captured using Hamamatsu ORCA R2 C10600 digital camera and
663 Metamorph software. For analysis of the number of myelin profiles in control vs mutant sciatic
664 nerves, semi-thin sections from proximal-, mid- and distal regions of the sciatic nerve were
665 taken, and 2 non- overlapping images of each section were obtained using the 60x objective. For
666 electron microscopy, stained ultrathin sections were examined using a JEOL 1010 electron
667 microscope fitted with a Hamamatsu digital camera and AMT Advantage image capture
668 software.
669
670 **Proliferation assays**

671 The percentage of Schwann cells in S-phase was measured by EdU incorporation. Mice were
672 injected intraperitoneally and subcutaneously with 80 μg/ g body weight of EdU dissolved in
673 PBS. Eighty minutes later, mice were sacrificed, and sciatic nerves removed and fixed for 1 hr.
674 in 4% paraformaldehyde; longitudinal 7μm cryosections were used for analysis. EdU
675 incorporation was identified using the Click-iT EdU Alexa Fluor 555 labeling kit (Molecular
676 Probes); the recommended protocol was followed, and labeling was for 1 hr. After EdU labeling,
677 sections were immunostained with anti-Sox10 to identify Schwann cells. The percentage of
678 Schwann cells (Sox10+ nuclei) that were EdU+ was determined by counting confocal images
679 using ImageJ software.
680
681 **Electrophysiology**
682 The procedure for measuring nerve conduction velocity was an adaption of a previously used
683 protocol (Schulz et al., 2014). Mice were deeply anesthetized, and hair was completely removed
684 from the hindquarters. A 27g percutaneous needle electrode was inserted subcutaneously over
685 the femur to stimulate the sciatic nerve at two locations: one proximal to the spinal cord, at the
686 hip joint, and the other 1cm distal to this site. The stimulation reference electrode (26G
687 percutaneous needle) was inserted over the back. Bipolar EMG electrodes were inserted
688 subcutaneously in the digital interosseous muscles, to record compound action potentials in
689 response to activation of the sciatic nerve. Stimulation and recording were conducted on both
690 hindlimbs. The muscle response was first tested with single pulses (100 μs duration) to
691 determine the threshold and level of activation producing a stable compound action potential in
692 the muscle. The level of stimulation which produced stable responses was then used for two
693 series of stimulations with 2-20s long trains of biphasic square wave pulses (100 μs duration)
694 delivered at 1-5 Hz. The nerve was rested for 2 minutes between runs. Stimulation was delivered
695 via an isolated pulse stimulator (A-M Systems Model 2100, A-M Systems Inc, Carlsborg, WA).
696 EMG compound muscle action potential (CMAP) responses were recorded with a differential
697 AC amplifier (A-M Systems Model 1700; gain 1k-10k; pass band 10-50 KHz). Data was
698 sampled at 50 KHz using LabVIEW (National Instruments Corporation, Austin, TX) running on
699 a personal computer. Multiple recordings were taken at each location to ensure a minimum of 10
700 representative responses for each location and animal. Electrophysiological data were analyzed
701 using Igor Pro (Wavemetrics Inc, Lake Oswego, OR).

702

703 **Data Analysis**

704 In each experiment, data collection and analysis were performed identically, regardless of mouse
705 genotype. Data are presented as mean +/- SD. Statistical analysis was done using the student's
706 unpaired t-test for two-group comparisons and analysis of variance (ANOVA) with Tukey's test
707 for multiple comparisons, according to the number of samples and the analysis of mice at
708 multiple ages. Sample sizes were similar to those conventional in the field and are indicated in
709 the main text, methods, or figure legends. A p-value of 0.05 or less was considered statistically
710 significant.

711

712 **SUPPLMENTARY MATERIALS**

713

714 **Supplementary figure 1. Additional semi-thin and TEM images of WT and *Tead1* cKO**

715 **(A)** Representative images of semi-thin sections of various areas of WT and Tead1 cKO SNs at
716 P22 and P50. Scale bar: 20μm

717 **(B)** Representative TEM images of transverse sections of WT and Tead1 cKO SNs at P22 and
718 P50. Scale bar: 1μm (P22 panels), 2μm (P50 panels)

719

720 **Supplementary video 1. A movie showing a P55 WT and two littermates *Tead1* cKO mice**

721

722 **REFERENCES AND NOTES**

723

724 Beirowski, B., Babetto, E., Golden, J.P., Chen, Y.J., Yang, K., Gross, R.W., Patti, G.J., and
725 Milbrandt, J. (2014). Metabolic regulator LKB1 is crucial for Schwann cell-mediated axon
726 maintenance. Nat Neurosci *17*, 1351-1361.

727 Beverdam, A., Claxton, C., Zhang, X., James, G., Harvey, K.F., and Key, B. (2013). Yap controls
728 stem/progenitor cell proliferation in the mouse postnatal epidermis. J Invest Dermatol *133*, 1497-
729 1505.

730 Bremer, M., Frob, F., Kichko, T., Reeh, P., Tamm, E.R., Suter, U., and Wegner, M. (2011). Sox10
731 is required for Schwann-cell homeostasis and myelin maintenance in the adult peripheral nerve.
732 Glia *59*, 1022-1032.

733 Clemence, A., Mirsky, R., and Jessen, K.R. (1989). Non-myelin-forming Schwann cells proliferate
734 rapidly during Wallerian degeneration in the rat sciatic nerve. J Neurocytol *18*, 185-192.

735 Currey, L., Thor, S., and Piper, M. (2021). TEAD family transcription factors in development and
736 disease. Development *148*.

737 Decker, L., Desmarquet-Trin-Dinh, C., Taillebourg, E., Ghislain, J., Vallat, J.M., and Charnay, P.
738 (2006). Peripheral myelin maintenance is a dynamic process requiring constant Krox20 expression.
739 The Journal of neuroscience : the official journal of the Society for Neuroscience *26*, 9771-9779.
740 Deng, Y., Wu, L.M.N., Bai, S., Zhao, C., Wang, H., Wang, J., Xu, L., Sakabe, M., Zhou, W., Xin,
741 M.*, et al.* (2017). A reciprocal regulatory loop between TAZ/YAP and G-protein Galphas regulates
742 Schwann cell proliferation and myelination. Nat Commun *8*, 15161.
743 Diepenbruck, M., Waldmeier, L., Ivanek, R., Berninger, P., Arnold, P., van Nimwegen, E., and
744 Christofori, G. (2014). Tead2 expression levels control the subcellular distribution of Yap and Taz,
745 zyxin expression and epithelial-mesenchymal transition. J Cell Sci *127*, 1523-1536.
746 Feltri, M.L., D'Antonio, M., Previtali, S., Fasolini, M., Messing, A., and Wrabetz, L. (1999). P0-
747 Cre transgenic mice for inactivation of adhesion molecules in Schwann cells. Ann N Y Acad Sci
748 *883*, 116-123.
749 Feltri, M.L., Poitelon, Y., and Previtali, S.C. (2016). How Schwann Cells Sort Axons: New
750 Concepts. Neuroscientist *22*, 252-265.
751 Fernando, R.N., Cotter, L., Perrin-Tricaud, C., Berthelot, J., Bartolami, S., Pereira, J.A., Gonzalez,
752 S., Suter, U., and Tricaud, N. (2016). Optimal myelin elongation relies on YAP activation by
753 axonal growth and inhibition by Crb3/Hippo pathway. Nat Commun *7*, 12186.
754 Finzsch, M., Schreiner, S., Kichko, T., Reeh, P., Tamm, E.R., Bosl, M.R., Meijer, D., and Wegner,
755 M. (2010). Sox10 is required for Schwann cell identity and progression beyond the immature
756 Schwann cell stage. J Cell Biol *189*, 701-712.
757 Gerber, D., Pereira, J.A., Gerber, J., Tan, G., Dimitrieva, S., Yángüez, E., and Suter, U. (2021).
758 Transcriptional profiling of mouse peripheral nerves to the single-cell level to build a sciatic nerve
759 ATlas (SNAT). Elife *10*.
760 Ghislain, J., and Charnay, P. (2006). Control of myelination in Schwann cells: a Krox20 cis-
761 regulatory element integrates Oct6, Brn2 and Sox10 activities. EMBO Rep *7*, 52-58.
762 Gomez-Sanchez, J.A., Lopez de Armentia, M., Lujan, R., Kessaris, N., Richardson, W.D., and
763 Cabedo, H. (2009). Sustained axon-glial signaling induces Schwann cell hyperproliferation,
764 Remak bundle myelination, and tumorigenesis. The Journal of neuroscience : the official journal
765 of the Society for Neuroscience *29*, 11304-11315.
766 Grove, M., Kim, H., Santerre, M., Krupka, A.J., Han, S.B., Zhai, J., Cho, J.Y., Park, R., Harris,
767 M., Kim, S.*, et al.* (2017). YAP/TAZ initiate and maintain Schwann cell myelination. Elife *6*.
768 Grove, M., Lee, H., Zhao, H., and Son, Y.J. (2020). Axon-dependent expression of YAP/TAZ
769 mediates Schwann cell remyelination but not proliferation after nerve injury. Elife *9*.
770 Harty, B.L., and Monk, K.R. (2017). Unwrapping the unappreciated: recent progress in Remak
771 Schwann cell biology. Current opinion in neurobiology *47*, 131-137.
772 He, X., Zhang, L., Queme, L.F., Liu, X., Lu, A., Waclaw, R.R., Dong, X., Zhou, W., Kidd, G.,
773 Yoon, S.O.*, et al.* (2018). A histone deacetylase 3-dependent pathway delimits peripheral myelin
774 growth and functional regeneration. Nature medicine *24*, 338-351.
775 He, Y., Kim, J.Y., Dupree, J., Tewari, A., Melendez-Vasquez, C., Svaren, J., and Casaccia, P.
776 (2010). Yy1 as a molecular link between neuregulin and transcriptional modulation of peripheral
777 myelination. Nat Neurosci *13*, 1472-1480.
778 Heinz, S., Romanoski, C.E., Benner, C., and Glass, C.K. (2015). The selection and function of cell
779 type-specific enhancers. Nat Rev Mol Cell Biol *16*, 144-154.
780 Hindley, C., and Philpott, A. (2012). Co-ordination of cell cycle and differentiation in the
781 developing nervous system. Biochem J *444*, 375-382.

782 Holden, J.K., and Cunningham, C.N. (2018). Targeting the Hippo Pathway and Cancer through
783 the TEAD Family of Transcription Factors. Cancers (Basel) *10*.
784 Hu, J.K., Du, W., Shelton, S.J., Oldham, M.C., DiPersio, C.M., and Klein, O.D. (2017). An FAK-
785 YAP-mTOR Signaling Axis Regulates Stem Cell-Based Tissue Renewal in Mice. Cell Stem Cell
786 *21*, 91-106 e106.
787 Jaegle, M., Ghazvini, M., Mandemakers, W., Piirsoo, M., Driegen, S., Levavasseur, F.,
788 Raghoenath, S., Grosveld, F., and Meijer, D. (2003). The POU proteins Brn-2 and Oct-6 share
789 important functions in Schwann cell development. Genes Dev *17*, 1380-1391.
790 Jang, S.W., Srinivasan, R., Jones, E.A., Sun, G., Keles, S., Krueger, C., Chang, L.W., Nagarajan,
791 R., and Svaren, J. (2010). Locus-wide identification of Egr2/Krox20 regulatory targets in myelin
792 genes. J Neurochem *115*, 1409-1420.
793 Jang, S.W., and Svaren, J. (2009). Induction of myelin protein zero by early growth response 2
794 through upstream and intragenic elements. J Biol Chem *284*, 20111-20120.
795 Jeanette, H., Marziali, L.N., Bhatia, U., Hellman, A., Herron, J., Kopec, A.M., Feltri, M.L.,
796 Poitelon, Y., and Belin, S. (2021). YAP and TAZ regulate Schwann cell proliferation and
797 differentiation during peripheral nerve regeneration. Glia *69*, 1061-1074.
798 Jessen, K.R., and Mirsky, R. (2005). The origin and development of glial cells in peripheral nerves.
799 Nat Rev Neurosci *6*, 671-682.
800 Jessen, K.R., and Mirsky, R. (2016). The repair Schwann cell and its function in regenerating
801 nerves. J Physiol *594*, 3521-3531.
802 Jones, E.A., Jang, S.W., Mager, G.M., Chang, L.W., Srinivasan, R., Gokey, N.G., Ward, R.M.,
803 Nagarajan, R., and Svaren, J. (2007). Interactions of Sox10 and Egr2 in myelin gene regulation.
804 Neuron Glia Biol *3*, 377-387.
805 Kao, S.C., Wu, H., Xie, J., Chang, C.P., Ranish, J.A., Graef, I.A., and Crabtree, G.R. (2009).
806 Calcineurin/NFAT signaling is required for neuregulin-regulated Schwann cell differentiation.
807 Science *323*, 651-654.
808 Kim, J., Kwon, H., Shin, Y.K., Song, G., Lee, T., Kim, Y., Jeong, W., Lee, U., Zhang, X., Nam,
809 G.*, et al.* (2020). MAML1/2 promote YAP/TAZ nuclear localization and tumorigenesis. Proc Natl
810 Acad Sci U S A *117*, 13529-13540.
811 Kim, M., Kim, T., Johnson, R.L., and Lim, D.S. (2015). Transcriptional co-repressor function of
812 the hippo pathway transducers YAP and TAZ. Cell Rep *11*, 270-282.
813 Kim, M., Wende, H., Walcher, J., Kuhnemund, J., Cheret, C., Kempa, S., McShane, E., Selbach,
814 M., Lewin, G.R., and Birchmeier, C. (2018). Maf links Neuregulin1 signaling to cholesterol
815 synthesis in myelinating Schwann cells. Genes Dev *32*, 645-657.
816 Kofler, M., Speight, P., Little, D., Di Ciano-Oliveira, C., Szaszi, K., and Kapus, A. (2018).
817 Mediated nuclear import and export of TAZ and the underlying molecular requirements. Nature
818 communications *9*, 4966.
819 Le, N., Nagarajan, R., Wang, J.Y., Araki, T., Schmidt, R.E., and Milbrandt, J. (2005a). Analysis
820 of congenital hypomyelinating Egr2Lo/Lo nerves identifies Sox2 as an inhibitor of Schwann cell
821 differentiation and myelination. Proc Natl Acad Sci U S A *102*, 2596-2601.
822 Le, N., Nagarajan, R., Wang, J.Y., Svaren, J., LaPash, C., Araki, T., Schmidt, R.E., and Milbrandt,
823 J. (2005b). Nab proteins are essential for peripheral nervous system myelination. Nat Neurosci *8*,
824 932-940.
825 LeBlanc, S.E., Jang, S.W., Ward, R.M., Wrabetz, L., and Svaren, J. (2006). Direct regulation of
826 myelin protein zero expression by the Egr2 transactivator. J Biol Chem *281*, 5453-5460.

827 Leblanc, S.E., Srinivasan, R., Ferri, C., Mager, G.M., Gillian-Daniel, A.L., Wrabetz, L., and
828 Svaren, J. (2005). Regulation of cholesterol/lipid biosynthetic genes by Egr2/Krox20 during
829 peripheral nerve myelination. J Neurochem *93*, 737-748.
830 Leone, D.P., Genoud, S., Atanasoski, S., Grausenburger, R., Berger, P., Metzger, D., Macklin,
831 W.B., Chambon, P., and Suter, U. (2003). Tamoxifen-inducible glia-specific Cre mice for somatic
832 mutagenesis in oligodendrocytes and Schwann cells. Mol Cell Neurosci *22*, 430-440.
833 Liu, R., Jagannathan, R., Li, F., Lee, J., Balasubramanyam, N., Kim, B.S., Yang, P., Yechoor,
834 V.K., and Moulik, M. (2019). Tead1 is required for perinatal cardiomyocyte proliferation. PloS
835 one *14*, e0212017.
836 Lopez-Anido, C., Poitelon, Y., Gopinath, C., Moran, J.J., Ma, K.H., Law, W.D., Antonellis, A.,
837 Feltri, M.L., and Svaren, J. (2016). Tead1 regulates the expression of Peripheral Myelin Protein
838 22 during Schwann cell development. Hum Mol Genet.
839 Lopez-Anido, C., Sun, G., Koenning, M., Srinivasan, R., Hung, H.A., Emery, B., Keles, S., and
840 Svaren, J. (2015). Differential Sox10 genomic occupancy in myelinating glia. Glia.
841 Meng, Z., Moroishi, T., and Guan, K.L. (2016). Mechanisms of Hippo pathway regulation. Genes
842 Dev *30*, 1-17.
843 Montani, L., Pereira, J.A., Norrmen, C., Pohl, H.B.F., Tinelli, E., Trotzmuller, M., Figlia, G.,
844 Dimas, P., von Niederhausern, B., Schwager, R.*, et al.* (2018). De novo fatty acid synthesis by
845 Schwann cells is essential for peripheral nervous system myelination. J Cell Biol *217*, 1353-1368.
846 Monuki, E.S., Kuhn, R., and Lemke, G. (1993). Repression of the myelin P0 gene by the POU
847 transcription factor SCIP. Mech Dev *42*, 15-32.
848 Mukhtar, T., Breda, J., Grison, A., Karimaddini, Z., Grobecker, P., Iber, D., Beisel, C., van
849 Nimwegen, E., and Taylor, V. (2020). Tead transcription factors differentially regulate cortical
850 development. Scientific reports *10*, 4625.
851 Norrmen, C., Figlia, G., Lebrun-Julien, F., Pereira, J.A., Trotzmuller, M., Kofeler, H.C., Rantanen,
852 V., Wessig, C., van Deijk, A.L., Smit, A.B.*, et al.* (2014). mTORC1 controls PNS myelination
853 along the mTORC1-RXRgamma-SREBP-lipid biosynthesis axis in Schwann cells. Cell Rep *9*,
854 646-660.
855 Norrmén, C., Figlia, G., Pfistner, P., Pereira, J.A., Bachofner, S., and Suter, U. (2018). mTORC1
856 Is Transiently Reactivated in Injured Nerves to Promote c-Jun Elevation and Schwann Cell
857 Dedifferentiation. The Journal of neuroscience : the official journal of the Society for
858 Neuroscience *38*, 4811-4828.
859 Poitelon, Y., Lopez-Anido, C., Catignas, K., Berti, C., Palmisano, M., Williamson, C., Ameroso,
860 D., Abiko, K., Hwang, Y., Gregorieff, A.*, et al.* (2016). YAP and TAZ control peripheral
861 myelination and the expression of laminin receptors in Schwann cells. Nat Neurosci *19*, 879-887.
862 Rasi, K., Hurskainen, M., Kallio, M., Staven, S., Sormunen, R., Heape, A.M., Avila, R.L.,
863 Kirschner, D., Muona, A., Tolonen, U.*, et al.* (2010). Lack of collagen XV impairs peripheral
864 nerve maturation and, when combined with laminin-411 deficiency, leads to basement membrane
865 abnormalities and sensorimotor dysfunction. J Neurosci *30*, 14490-14501.
866 Ren, B., and Yue, F. (2015). Transcriptional Enhancers: Bridging the Genome and Phenome. Cold
867 Spring Harb Symp Quant Biol *80*, 17-26.
868 Ryu, E.J., Wang, J.Y., Le, N., Baloh, R.H., Gustin, J.A., Schmidt, R.E., and Milbrandt, J. (2007).
869 Misexpression of Pou3f1 results in peripheral nerve hypomyelination and axonal loss. J Neurosci
870 *27*, 11552-11559.

871 Saher, G., Quintes, S., Mobius, W., Wehr, M.C., Kramer-Albers, E.M., Brugger, B., and Nave,
872 K.A. (2009). Cholesterol regulates the endoplasmic reticulum exit of the major membrane protein
873 P0 required for peripheral myelin compaction. J Neurosci *29*, 6094-6104.
874 Salzer, J.L. (2015). Schwann cell myelination. Cold Spring Harb Perspect Biol *7*, a020529.
875 Scherer, S.S., and Wrabetz, L. (2008). Molecular mechanisms of inherited demyelinating
876 neuropathies. Glia *56*, 1578-1589.
877 Schulz, A., Walther, C., Morrison, H., and Bauer, R. (2014). In vivo electrophysiological
878 measurements on mouse sciatic nerves. J Vis Exp.
879 Sherman, D.L., Krols, M., Wu, L.M., Grove, M., Nave, K.A., Gangloff, Y.G., and Brophy, P.J.
880 (2012). Arrest of myelination and reduced axon growth when Schwann cells lack mTOR. The
881 Journal of neuroscience : the official journal of the Society for Neuroscience *32*, 1817-1825.
882 Son, Y.J., and Thompson, W.J. (1995). Schwann cell processes guide regeneration of peripheral
883 axons. Neuron *14*, 125-132.
884 Taveggia, C., Zanazzi, G., Petrylak, A., Yano, H., Rosenbluth, J., Einheber, S., Xu, X., Esper,
885 R.M., Loeb, J.A., Shrager, P.*, et al.* (2005). Neuregulin-1 type III determines the ensheathment
886 fate of axons. Neuron *47*, 681-694.
887 Topilko, P., Schneider-Maunoury, S., Levi, G., Baron-Van Evercooren, A., Chennoufi, A.B.,
888 Seitanidou, T., Babinet, C., and Charnay, P. (1994). Krox-20 controls myelination in the peripheral
889 nervous system. Nature *371*, 796-799.
890 Tricaud, N., and Park, H.T. (2017). Wallerian demyelination: chronicle of a cellular cataclysm.
891 Cell Mol Life Sci *74*, 4049-4057.
892 Varelas, X. (2014). The Hippo pathway effectors TAZ and YAP in development, homeostasis and
893 disease. Development *141*, 1614-1626.
894 Verheijen, M.H., Camargo, N., Verdier, V., Nadra, K., de Preux Charles, A.S., Medard, J.J.,
895 Luoma, A., Crowther, M., Inouye, H., Shimano, H.*, et al.* (2009). SCAP is required for timely and
896 proper myelin membrane synthesis. Proc Natl Acad Sci U S A *106*, 21383-21388.
897 Wen, T., Liu, J., He, X., Dong, K., Hu, G., Yu, L., Yin, Q., Osman, I., Peng, J., Zheng, Z.*, et al.*
898 (2019). Transcription factor TEAD1 is essential for vascular development by promoting vascular
899 smooth muscle differentiation. Cell death and differentiation *26*, 2790-2806.
900 Wen, T., Yin, Q., Yu, L., Hu, G., Liu, J., Zhang, W., Huang, L., Su, H., Wang, M., and Zhou, J.
901 (2017). Characterization of mice carrying a conditional TEAD1 allele. Genesis (New York, NY :
902 2000) *55*.
903 Wright, M.C., Cho, W.J., and Son, Y.J. (2007). Distinct patterns of motor nerve terminal sprouting
904 induced by ciliary neurotrophic factor vs. botulinum toxin. J Comp Neurol *504*, 1-16.
905 Xiao, J.H., Davidson, I., Matthes, H., Garnier, J.M., and Chambon, P. (1991). Cloning, expression,
906 and transcriptional properties of the human enhancer factor TEF-1. Cell *65*, 551-568.
907 Yao, F., Zhou, Z., Kim, J., Hang, Q., Xiao, Z., Ton, B.N., Chang, L., Liu, N., Zeng, L., Wang, W.,
908 *et al.* (2018). SKP2- and OTUD1-regulated non-proteolytic ubiquitination of YAP promotes YAP
909 nuclear localization and activity. Nature communications *9*, 2269.
910 Zheng, Y., and Pan, D. (2019). The Hippo Signaling Pathway in Development and Disease.
911 Developmental cell *50*, 264-282.
912 Zorick, T.S., Syroid, D.E., Brown, A., Gridley, T., and Lemke, G. (1999). Krox-20 controls SCIP
913 expression, cell cycle exit and susceptibility to apoptosis in developing myelinating Schwann cells.
914 Development *126*, 1397-1406.
915

916

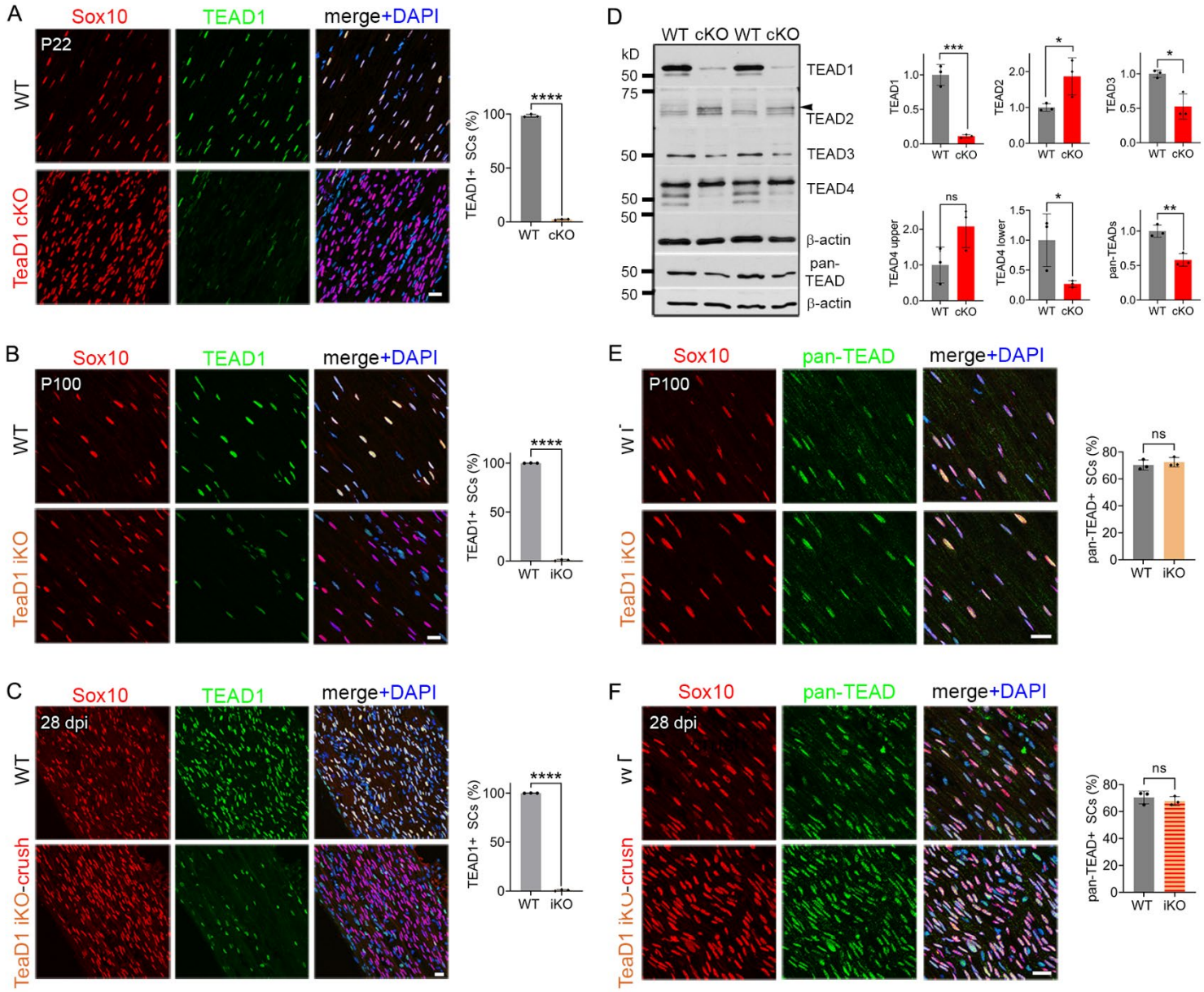

Figure 1. Expression of TEADs in Schwann cells (SCs) of WT, *Tead1* cKO, and iKO mice

(A) Immunostaining and quantification of TEAD1+ SCs on longitudinal sections of P22 WT and *Tead1* cKO SNs. SC nuclei are identified by Sox10. All cell nuclei are marked by DAPI. n = 3 mice per genotype, ****P < 0.0001, Student's unpaired t-test. Scale bar: 20μm

924 **(B)** Immunostaining and quantification of TEAD1+ SCs on longitudinal sections of WT and
925 *Tead1* iKO SNs 3 months after tamoxifen administration. SC nuclei are identified by Sox10. All
926 cell nuclei are marked by DAPI. n = 3 mice per genotype, ****P < 0.0001, Student's unpaired t-
927 test. Scale bar: 20μm
928 **(C)** Immunostaining and quantification of TEAD1+ SCs on longitudinal sections of WT and
929 *Tead1* iKO SNs 28 days after nerve crush. SC nuclei are identified by Sox10. All cell nuclei are
930 marked by DAPI. n = 3 mice per genotype, ****P < 0.0001, Student's unpaired t-test. Scale bar:
931 20μm
932 **(D)** Western blotting of P50 WT and *Tead1* cKO SN lysates with anti-TEAD1, -TEAD2, -
933 TEAD3, -TEAD4, and -pan TEAD. TEAD expression is normalized to that of *β-actin* as an
934 internal control, and WT expression is arbitrarily given the value 1. n = 3 mice per genotype. ns,
935 p > 0.05; *p ≤ 0.05, **p ≤ 0.005, ***p ≤ 0.001, unpaired Student's t-test.
936 **(E)** Immunostaining and quantification of pan-TEAD+ SCs on longitudinal sections of P100 WT
937 and *Tead1* iKO SNs. SC nuclei are identified by Sox10. All cell nuclei are marked by DAPI. n =
938 3 mice per genotype. ns, p > 0.05, Student's unpaired t-test. Scale bar: 20μm
939 **(F)** Immunostaining and quantification of pan-TEAD+ SCs on longitudinal sections of P100 WT
940 and *Tead1* iKO SNs 28 days after nerve crush. SC nuclei are identified by Sox10. All cell nuclei
941 are marked by DAPI. n = 3 mice per genotype. ns, p > 0.05, Student's unpaired t-test. Scale bar:
942 20μm

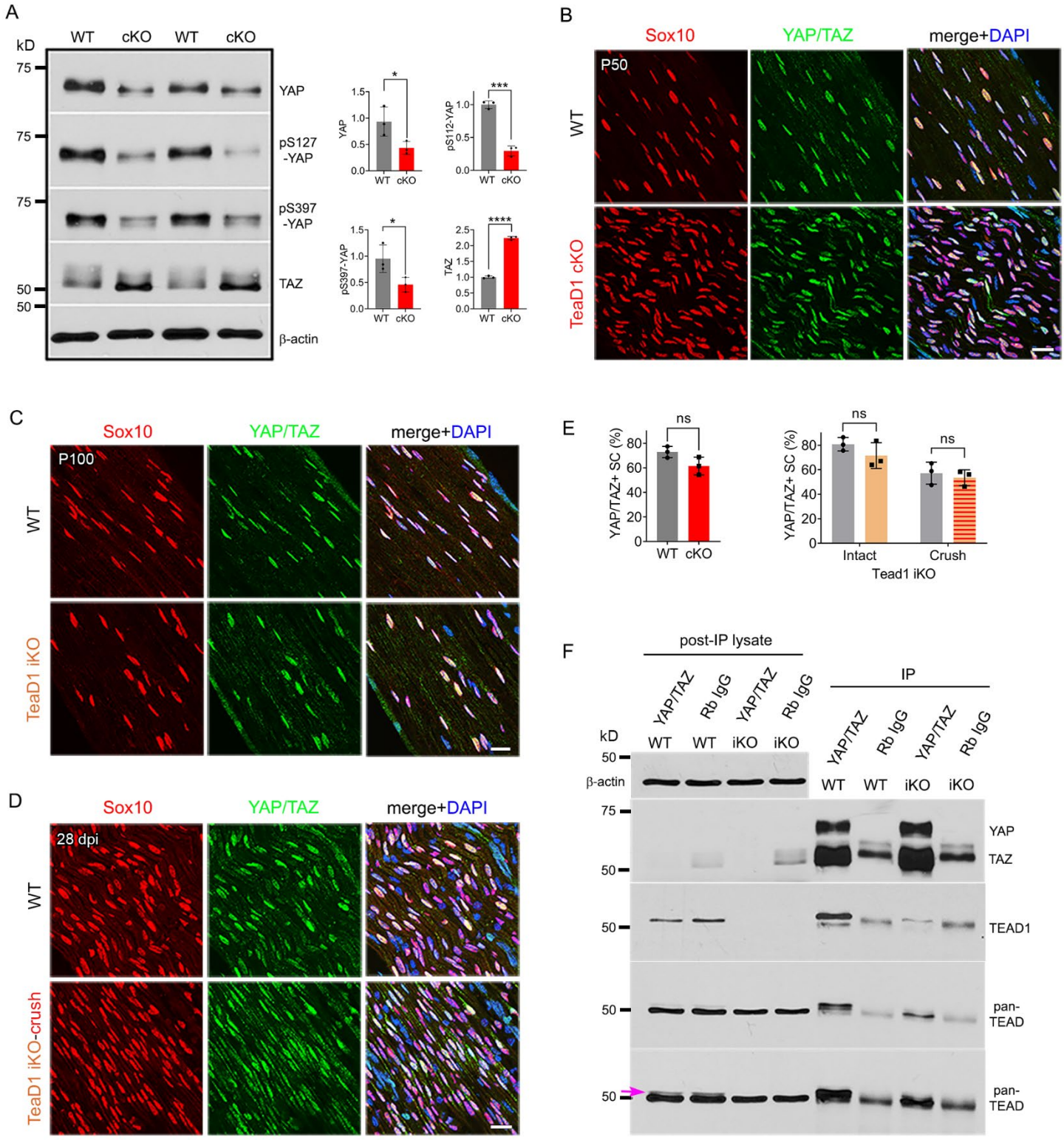

943

944 **Figure 2. YAP/TAZ strongly favor TEAD1 but partner with other TEADs**

945 **(A)** Western blotting of P50 WT and *Tead1* cKO SN lysates with anti-YAP, -phospho-YAPs
946 (Ser127 and Ser397), and -TAZ. YAP/TAZ expression is normalized to that of *β-actin* as an
947 internal control, and WT expression is arbitrarily given the value 1. n = 3 mice per genotype. *p
948 ≤ 0.05, ***p ≤ 0.001, ****P < 0.0001, Student's unpaired t-test.
949 **(B)** Immunostaining of YAP/TAZ+ SCs on longitudinal sections of P50 WT and *Tead1* cKO
950 SNs. SC nuclei are identified by Sox10. All cell nuclei are marked by DAPI. Scale bar: 20μm
951 **(C)** Immunostaining of YAP/TAZ+ SCs on longitudinal sections of P100 WT and *Tead1* iKO
952 SNs. SC nuclei are identified by Sox10. All cell nuclei are marked by DAPI. Scale bar: 20μm
953 **(D)** Immunostaining of YAP/TAZ+ SCs on longitudinal sections of P100 WT and *Tead1* iKO
954 SNs 28 days after nerve crush. SC nuclei are identified by Sox10. All cell nuclei are marked by
955 DAPI. Scale bar: 20μm
956 **(E)** Quantification of YAP/TAZ+ SCs in WT, Tead1 cKO, intact, and injured *Tead1* iKO SNs. n
957 = 3 mice per group. ns, p > 0.05, Student's unpaired t-test.
958 **(F)** Immunoprecipitation of P100 WT and *Tead1* iKO SN lysates with anti-YAP/TAZ and
959 control Rb IgG. Lysate samples, labeled post-IP lysate, were taken from tubes after
960 immunoprecipitated complexes attached to beads had been spun down to assess the efficiency.
961 Immunoprecipitates were blotted for YAP/TAZ, TEAD1, and pan-TEAD. Arrow denotes a faint
962 TEAD1 band revealed by pan-TEAD in WT lysate.
963

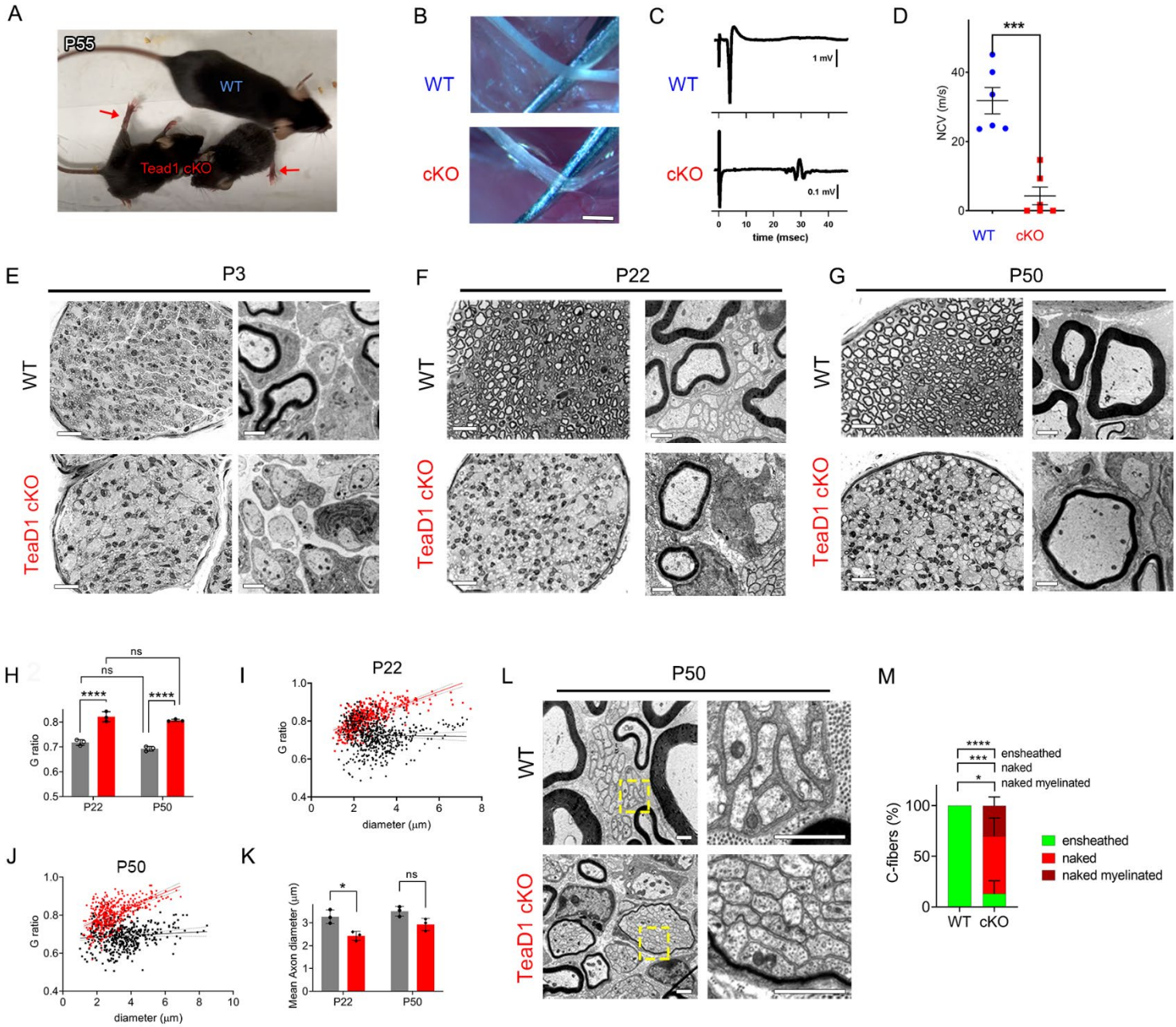

964

965 **Figure 3. TEAD1 is required for myelin sheath formation and growth**

966 **(A)** A living control (WT) and two *Tead1* cKO mice from one litter at P55. Arrows point to

967 splayed paralyzed hindlimbs.

968 **(B)** Exposed SNs of WT and *Tead1* cKO mice during dissection. Scale bar: 1mm

969 **(C)** Representative images of CMAPs generated by stimulation of WT and *Tead1* cKO SNs.

970 **(D)** Quantification of NCV in WT and *Tead1* cKO. n = 6 mice per genotype. ***P < 0.001,
971 Student's unpaired t-test.
972 **(E)** Representative images of semithin (left panels) and TEM (right panels) of transverse sections
973 of WT and *Tead1* cKO SNs at P3. Scale bar: 20μm (left panels), 1μm (right panels)
974 **(F)** Representative images of semithin (left panels) and TEM (right panels) of transverse sections
975 of WT and *Tead1* cKO SNs at P22. Scale bar: 20μm (left panels), 1μm (right panels)
976 **(G)** Representative images of semithin (left panels) and TEM (right panels) of transverse
977 sections of WT and *Tead1* cKO SNs at P50. Scale bar: 20μm (left panels), 1μm (right panels)
978 **(H)** Quantification of G-ratio for axons in WT and *Tead1* cKO SNs at P22 and at P50. n = 3
979 mice per group. ns, p > 0.05 (P22 WT versus P50 WT, P22 cKO versus P50 cKO), ****P <
980 0.0001 (P22 WT versus P22 cKO, P50 WT versus P50 cKO).
981 **(I)** Scatter plot graph displaying G-ratio in relation to axon diameter in WT and *Tead1* cKO SNs
982 at P22. n = 1063 axons from 3 mice per each genotype.
983 **(J)** Scatter plot graph displaying G-ratio in relation to axon diameter in WT and *Tead1* cKO SNs
984 at P50. n = 880 axons from 3 mice per each genotype.
985 **(K)** Quantitative comparison of mean axon diameter in WT and *Tead1* cKO SNs at P22 and at
986 P50. n = 3 mice per group. ns, p > 0.05, *p ≤ 0.05, 2-way ANOVA with Tukey's multiple
987 comparisons test.
988 **(L)** Representative TEM images of transverse sections of P50 WT and *Tead1* cKO SNs. Right
989 panels are enlarged images of the boxed area in left panels. Scale bar: 1μm
990 **(M)** Quantification of normal and abnormal C-fibers in P50 WT and *Tead1* cKO SNs. C-fibers
991 normally ensheathed by SC cytoplasm are marked as 'ensheathed', whereas those not ensheathed
992 are denoted as 'naked'. Naked C-fibers located in a myelinated bundle are denoted as 'naked
993 myelinated'. Relative percentage of each type of C-fiber is plotted. N > 500 C-fibers from 3 mice
994 per each genotype. *p ≤ 0.05, ***p ≤ 0.001, ****P < 0.0001, 2-way ANOVA Tukey's multiple
995 comparisons test.
996

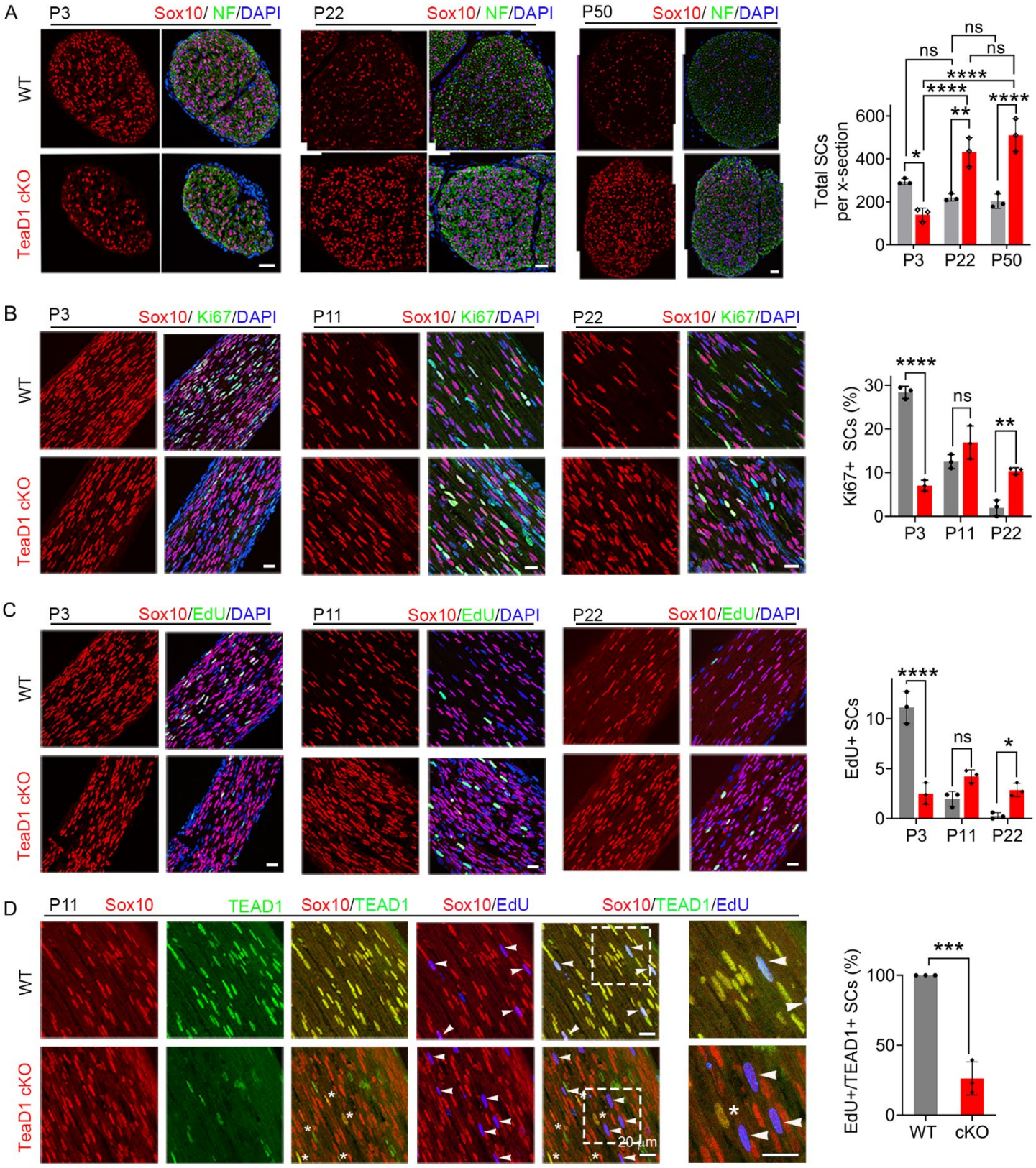
A
P3
Sox10/ NF/DAPI
P22
Sox10/ NF/DAPI
P50
Sox10/ NF/DAPI
WT
TeaD1 cKO
Total SCs per x-section
ns
ns
ns
****
****
****
**
*
P3
P22
P50
B
P3
Sox10/ Ki67/DAPI
P11
Sox10/ Ki67/DAPI
P22
Sox10/ Ki67/DAPI
WT
TeaD1 cKO
Ki67+ SCs (%)
****
ns
**
P3
P11
P22
C
P3
Sox10/EdU/DAPI
P11
Sox10/EdU/DAPI
P22
Sox10/EdU/DAPI
WT
TeaD1 cKO
EdU+ SCs
****
ns
*
P3
P11
P22
D
P11
Sox10
TEAD1
Sox10/TEAD1
Sox10/EdU
Sox10/TEAD1/EdU
WT
TeaD1 cKO
20 μm
EdU+/TEAD1+ SCs (%)
***
WT
cKO

997

998 **Figure 4. TEAD1 regulates SC proliferation both positively and negatively**

999 **(A)** Immunostaining and quantification of SCs on transverse sections of WT and *Tead1* iKO SNs
1000 at P3, P22, and P52. SC nuclei and all cell nuclei are marked by Sox10 and DAPI. Axons are
1001 marked by Neurofilaments (NF). n = 3 mice per genotype, ns, $p > 0.05$, *$p \leq 0.05$, **$p \leq 0.01$,
1002 ****$P < 0.0001$, 2-way ANOVA with Tukey's multiple comparisons test. Scale bar: 30μm

1003 **(B)** Immunostaining and quantification of Ki67+ SCs on longitudinal sections of WT and *Tead1*
1004 iKO SNs at P3, P11, and P22. SC nuclei and all cell nuclei are marked by Sox10 and DAPI. n =
1005 3 mice per genotype, ns, $p > 0.05$, **$p \leq 0.01$, ****$P < 0.0001$, 2-way ANOVA with Tukey's
1006 multiple comparisons test. Scale bar: 30μm (P3 panels), 20μm (P11 and P22 panels)

1007 **(C)** Immunostaining and quantification of EdU+ SCs on longitudinal sections of WT and *Tead1*
1008 iKO SNs at P3, P11, and P22. SC nuclei and all cell nuclei are marked by Sox10 and DAPI. n =
1009 3 mice per genotype, ns, $p > 0.05$, *$p \leq 0.05$, ****$P < 0.0001$, 2-way ANOVA with Tukey's
1010 multiple comparisons test. Scale bar: 30μm (P3 panels), 20μm (P11 and P22 panels)

1011 **(D)** Immunostaining and quantification of EdU+/TEAD1+ SCs on longitudinal sections of WT
1012 and *Tead1* iKO SNs at P11. SC nuclei are marked by Sox10. Asterisks denote *Tead1* cKO SCs in
1013 which TEAD1 is not deleted and which are not EdU+. Arrowheads denote EdU+ SCs which are
1014 TEAD1+ in WT but TEAD1- in *Tead1* cKO. n = 3 mice per genotype, ***$P < 0.001$, Student's
1015 unpaired t-test. Scale bar: 20μm

1016

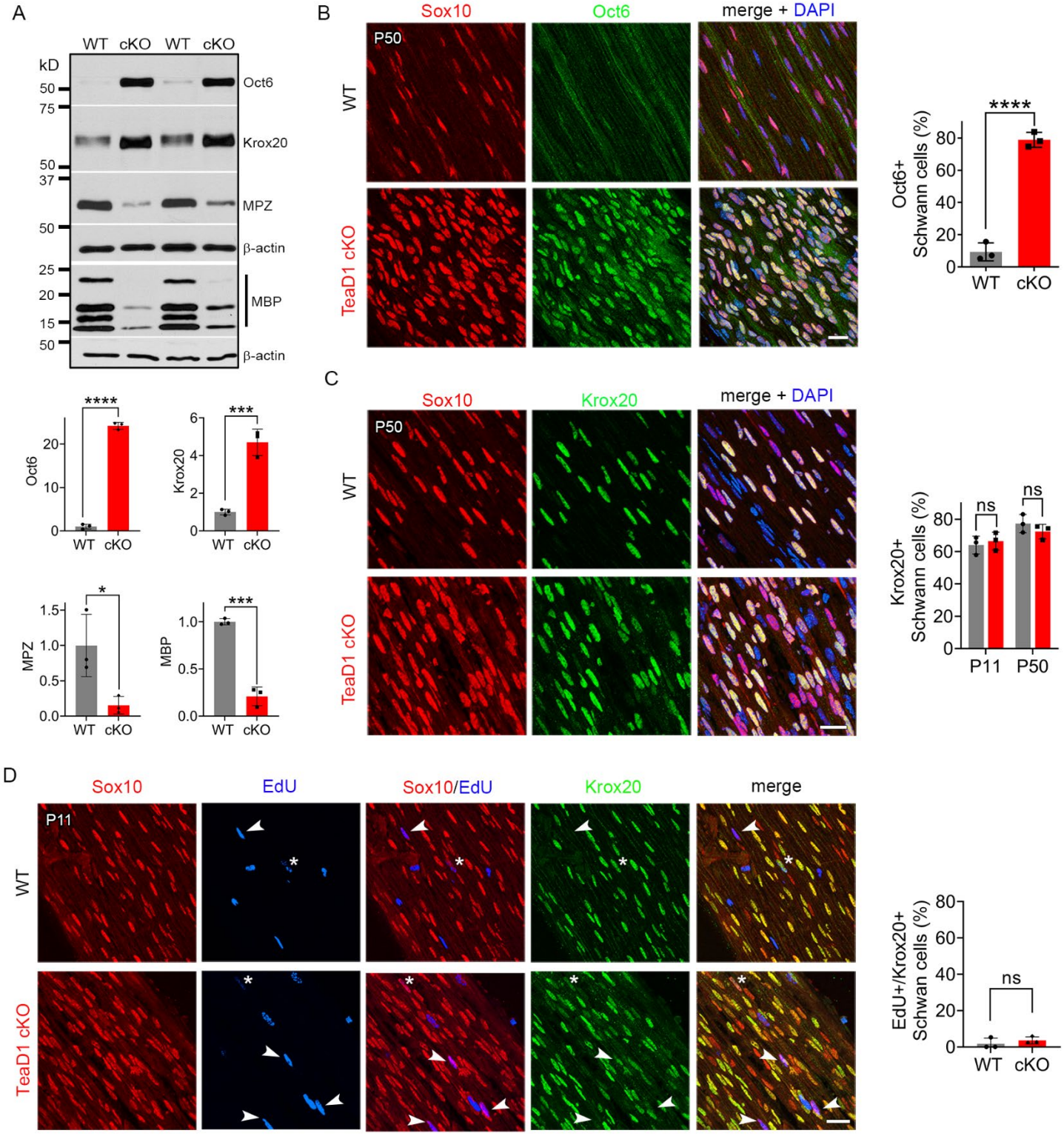
A
WT cKO WT cKO
kD
50
75
50
37
50
25
20
15
50
Oct6
Krox20
MPZ
β-actin
MBP
β-actin
Oct6
Krox20
MPZ
MBP
WT cKO
B
Sox10
Oct6
merge + DAPI
P50
WT
TeaD1 cKO
Oct6+ Schwann cells (%)
****
C
Sox10
Krox20
merge + DAPI
P50
WT
TeaD1 cKO
Krox20+ Schwann cells (%)
ns
P11 P50
D
Sox10
EdU
Sox10/EdU
Krox20
merge
P11
WT
TeaD1 cKO
EdU+/Krox20+ Schwan cells (%)
ns
WT cKO

1017

1018 **Figure 5. TEAD1 is required for Krox20 to upregulate myelin proteins during**
1019 **development**
1020 **(A)** Western blotting of P50 WT and *Tead1* cKO SN lysates with anti-Oct6, -Krox20, -MPZ, and
1021 -MBP. Protein expression is normalized to that of *β-actin* as an internal control, and WT
1022 expression is arbitrarily given the value 1. n = 3 mice per genotype. *$p \leq 0.05$, ***$p \leq 0.001$,
1023 ***$p \leq 0.0001$, Student's unpaired t-test.
1024 **(B)** Immunostaining and quantification of Oct6+ SCs on longitudinal sections of P50 WT and
1025 *Tead1* cKO SNs. SC nuclei are identified by Sox10. All cell nuclei are marked by DAPI. n = 3
1026 mice per genotype, ****$P < 0.0001$, Student's unpaired t-test. Scale bar: 20μm
1027 **(C)** Immunostaining and quantification of Krox20+ SCs on longitudinal sections of WT and
1028 *Tead1* cKO SNs at P11 and P50. SC nuclei are identified by Sox10. All cell nuclei are marked by
1029 DAPI. n = 3 mice per each group, ns, $p > 0.05$, Student's unpaired t-test. Scale bar: 20μm
1030 **(D)** Immunostaining and quantification of EdU+/Krox20+ SCs on longitudinal sections of WT
1031 and *Tead1* cKO SNs at P11. SC nuclei are identified by Sox10. Arrowheads denote examples of
1032 EdU+ SCs which are Krox20-. Asterisks denote rarely observed EdU+ SCs which are Krox20+.
1033 n = 3 mice per genotype, ns, $p > 0.05$, Student's unpaired t-test. Scale bar: 20μm
1034

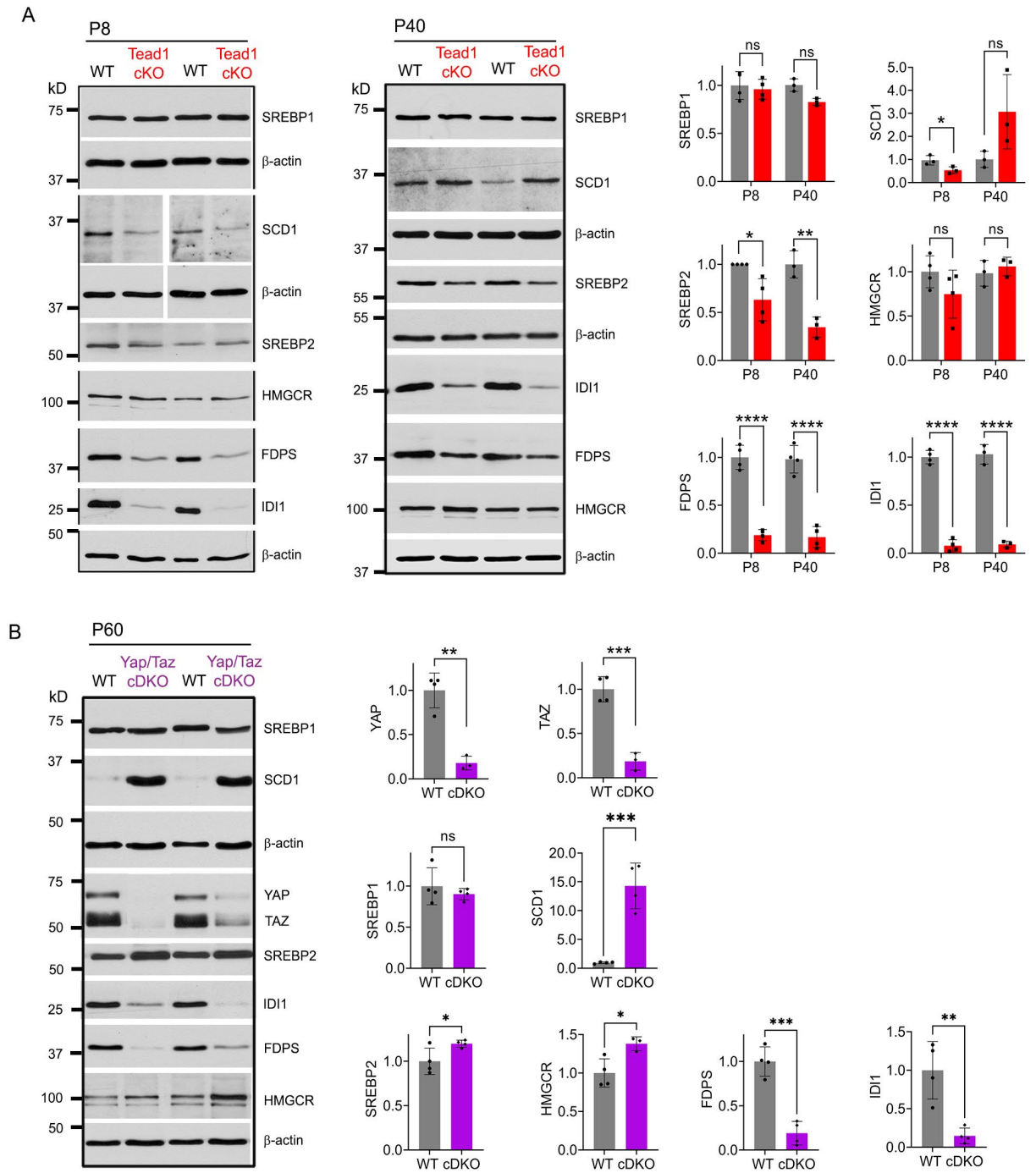

Figure 6. TEAD1 and YAP/TAZ upregulate cholesterol synthesis enzymes: FDPS and IDI1 **(A)** Western blotting of P8 and P40 WT and *Tead1* cKO SN lysates with anti-SREBP1, -SCD1, -SREBP2, -HMGCR, -FDPS, and -IDI1. Protein expression is normalized to that of *β-actin* as an internal control, and WT expression is arbitrarily given the value 1. n = 3 or 4 mice per genotype. ns, $p > 0.05$, *$p \leq 0.05$, **$p \leq 0.01$, ****$P < 0.0001$, Student's unpaired t-test. **(B)** Western

blotting of P60 WT and *Yap/Taz* cDKO SN lysates with anti-YAP, -TAZ, -SREBP1, -SCD1, -SREBP2, -HMGCR, -FDPS, and -IDI1. Protein expression is normalized to that of *β-actin* as an internal control, and WT expression is arbitrarily given the value 1. n = 3 or 4 mice per genotype. ns, $p > 0.05$, $*p \leq 0.05$, $**p \leq 0.01$, $***P < 0.001$, Student's unpaired t-test.

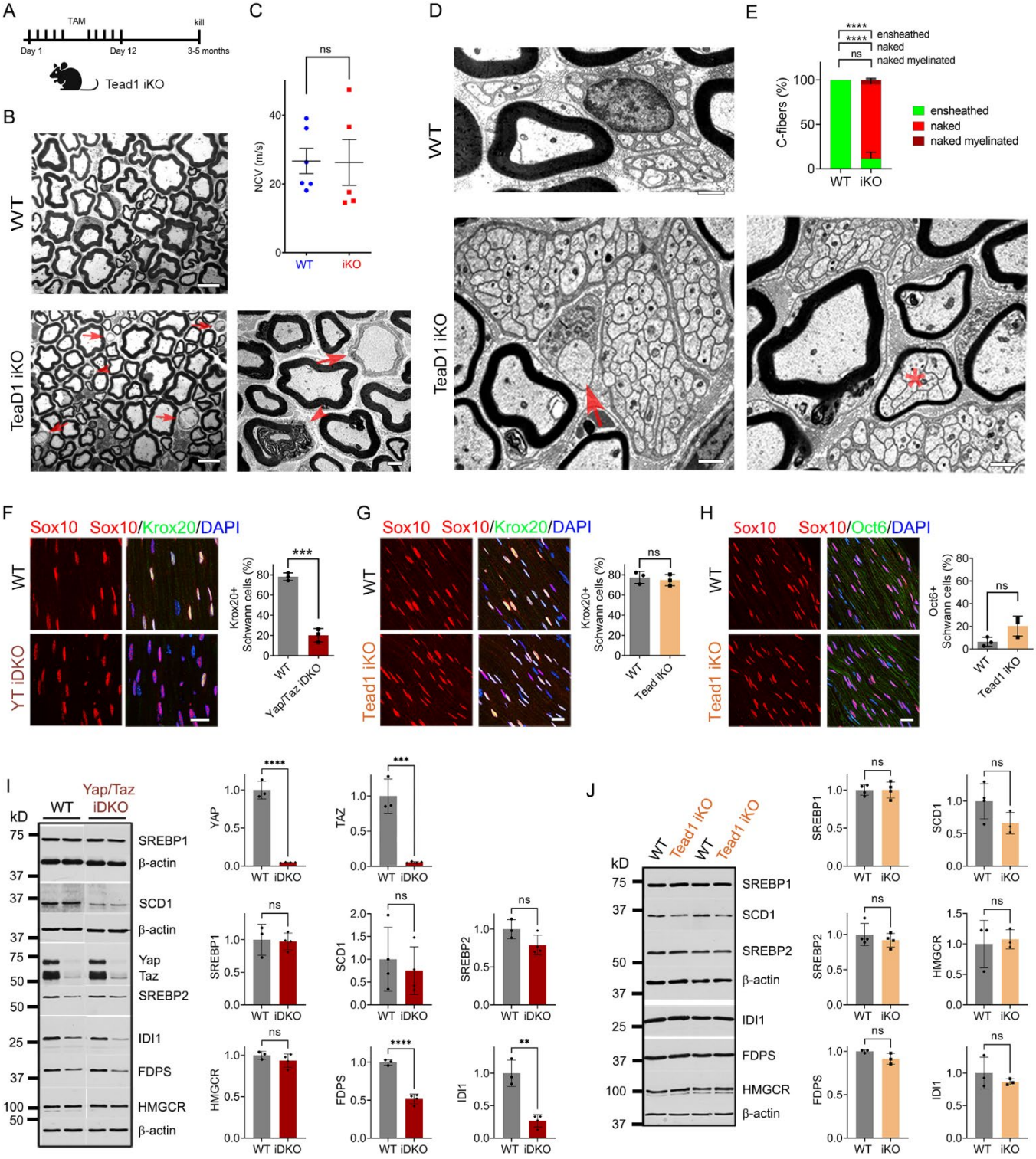

1045

1046 **Figure 7. TEAD1 is largely dispensable for myelin maintenance, but required for**
1047 **preservation of Remak bundle integrity**

1048 **(A)** Cartoon showing timeline of tamoxifen injection and time of sacrifice of *Tead1* iKO mice.

1049 **(B)** Representative TEM images of P150 WT and *Tead1* iKO SNs showing occasional large
1050 axons undergoing demyelination (arrowheads) or completely demyelinated (arrows). Scale bar:
1051 6μm (left panels), 2μm (right panel)

1052 **(C)** Quantification of NCV in P90-P150 WT and *Tead1* iKO mice. n = 5 or 6 mice per genotype.
1053 ns, $p > 0.05$, Student's unpaired t-test.

1054 **(D)** Representative TEM images of P97 WT and *Tead1* iKO SNs showing Remak bundles.
1055 Asterisk denotes a bundle of thinly myelinated C-fibers. Arrow denotes demyelinated axon.
1056 Scale bar: 1μm

1057 **(E)** Quantification of normal and abnormal C-fibers in P150 WT and *Tead1* iKO SNs. Relative
1058 percentage of each type of C-fiber is plotted. N > 500 C-fibers from 3 mice per each genotype.
1059 ns, $p > 0.05$, ****$P < 0.0001$, 2-way ANOVA Tukey's multiple comparisons test.

1060 **(F)** Immunostaining and quantification of Krox20+ SCs on longitudinal sections of WT and
1061 *Yap/Taz* iKO SNs 2 weeks after 1st tamoxifen injection. SC nuclei are marked by Sox10. All cell
1062 nuclei are marked by DAPI. n = 3 mice per genotype, ***$P < 0.001$, Student's unpaired t-test.
1063 Scale bar: 20μm

1064 **(G)** Immunostaining and quantification of Krox20+ SCs on longitudinal sections of WT and
1065 *Tead1* iKO SNs 6 weeks after 1st tamoxifen injection. SC nuclei are marked by Sox10. All cell
1066 nuclei are marked by DAPI. n = 3 mice per genotype, ns, $p > 0.05$, Student's unpaired t-test.
1067 Scale bar: 20μm

1068 **(H)** Immunostaining and quantification of Oct6+ SCs on longitudinal sections of WT and *Tead1*
1069 iKO SNs 6 weeks after 1st tamoxifen injection. SC nuclei are marked by Sox10. All cell nuclei
1070 are marked by DAPI. n = 3 mice per genotype, ns, $p > 0.05$, Student's unpaired t-test. Scale bar:
1071 20μm

1072 **(I)** Western blotting of WT and *Yap/Taz* iDKO SN lysates with anti-YAP, -TAZ, -SREBP1, -
1073 SCD1, -SREBP2, -HMGCR, -FDPS, and -IDI1. Protein expression is normalized to that of *β-*
1074 *actin* as an internal control, and WT expression is arbitrarily given the value 1. n = 3 or 4 mice
1075 per genotype. ns, $p > 0.05$, **$p \leq 0.01$, ***$P < 0.001$, ****$P < 0.0001$, Student's unpaired t-test.

1076 **(J)** Western blotting of WT and *Tead1* iKO SN lysates with anti-SREBP1, -SCD1, -SREBP2, -
1077 HMGCR, -FDPS, and -IDI1. Protein expression is normalized to that of *β-actin* as an internal
1078 control, and WT expression is arbitrarily given the value 1. n = 3 or 4 mice per genotype. ns, p >
1079 0.05, Student's unpaired t-test.
1080

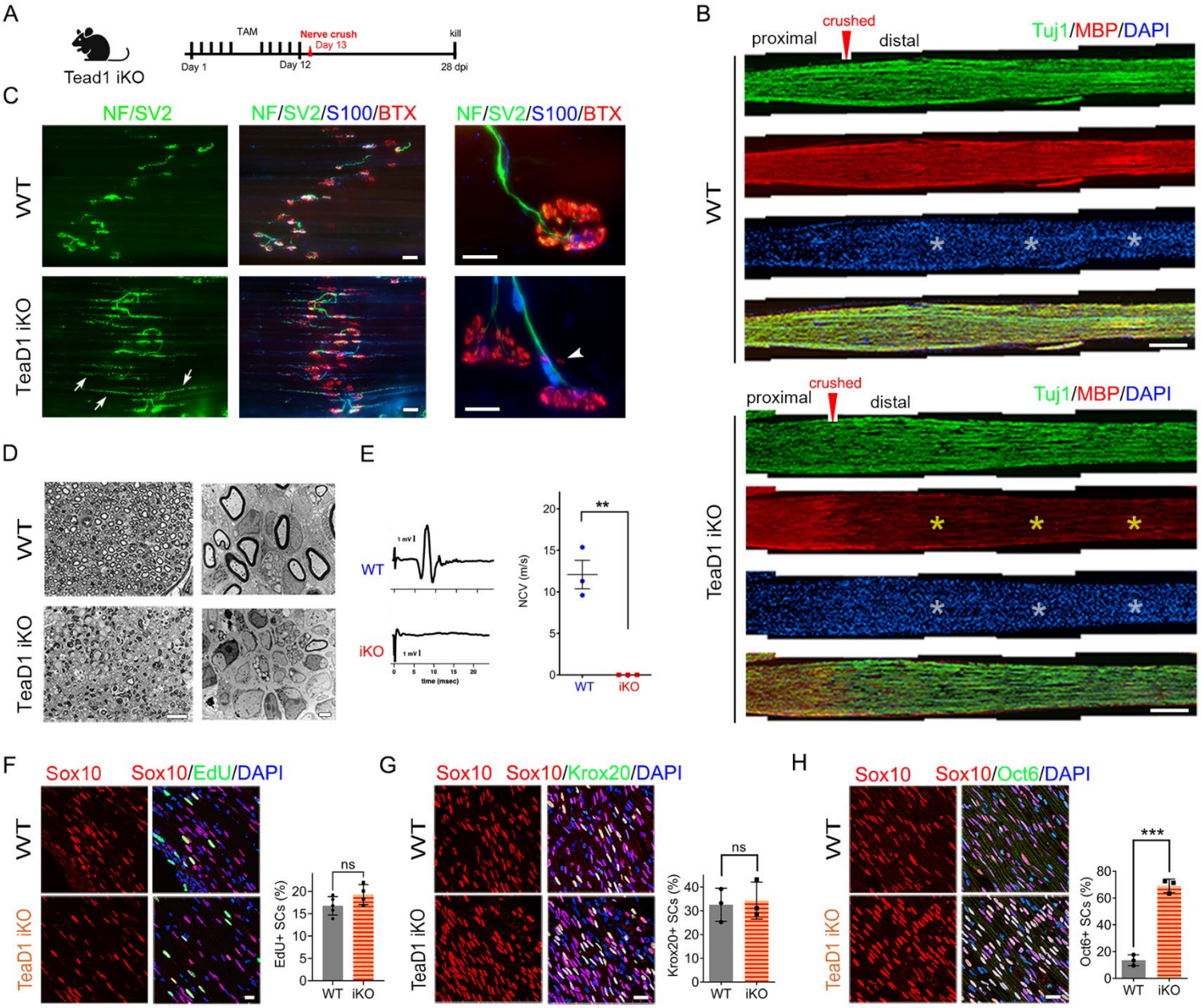

1081

1082 **Figure 8. TEAD1 is required for functional regeneration of peripheral nerve**

1083 **(A)** Cartoon showing timeline of tamoxifen injection and time of sacrifice of *Tead1* iKO mice
1084 after nerve crush.
1085 **(B)** Low magnification images of longitudinal sections of ~4mm long SN segments of WT and
1086 *Tead1* iKO mice 28 days after nerve crush. Arrowheads denote crush site. Axons and myelin are
1087 marked by Tuj1 and MBP, respectively. All cell nuclei are marked by DAPI. Yellow asterisks
1088 denote the distal nerve segment of *Tead1* iKO, which almost completely lacks myelin. White
1089 asterisks denote distal segments of both WT and *Tead1* iKO, which exhibit more cells than
1090 proximal segments due to SC proliferation after injury. Scale bar: 500μm
1091 **(C)** Representative low and high magnification NMJ images of WT and Tead1 iKO 28 days after
1092 nerve crush. Axon and axon terminals are marked by neurofilament (NF) and SV2 staining. SCs
1093 are marked by S100. Muscle acetylcholine receptors are marked by α-Bungarotoxin. Arrows
1094 denote examples of axon terminals that grew past NMJs in iKO. Arrowheads denote examples of
1095 extrasynaptic AChR clusters in iKO. Scale bar: 50μm (low magnification panels), 20μm (high
1096 magnification panels)
1097 **(D)** Representative semi-thin and TEM images of transverse sections of WT and *Tead1* iKO 28
1098 days after nerve crush. Scale bar: 20μm (left semi-thin panels), 2μm (right TEM panels)
1099 **(E)** Representative CMAP recordings and NCV measurements of WT and *Tead1* iKO at 28 days
1100 after nerve crush. n = 3 mice per genotype, **$p \leq 0.01$, Student's unpaired t-test.
1101 **(F)** Immunostaining and quantification of EdU+ SCs on longitudinal sections of WT and *Tead1*
1102 iKO SNs at 28 days after nerve crush. SC nuclei are marked by Sox10. All cell nuclei are marked
1103 by DAPI. n = 4 mice per genotype, ns, $p > 0.05$, Student's unpaired t-test. Scale bar: 20μm
1104 **(G)** Immunostaining and quantification of Krox20+ SCs on longitudinal sections of WT and
1105 *Tead1* iKO SNs at 28 days after nerve crush. SC nuclei are marked by Sox10. All cell nuclei are
1106 marked by DAPI. n = 3 mice per genotype, ns, $p > 0.05$, Student's unpaired t-test. Scale bar:
1107 20μm
1108 **(H)** Immunostaining and quantification of Oct6+ SCs on longitudinal sections of WT and *Tead1*
1109 iKO SNs at 28 days after nerve crush. SC nuclei are marked by Sox10. All cell nuclei are marked
1110 by DAPI. n = 3 mice per genotype, ns, ***$P < 0.001$, Student's unpaired t-test. Scale bar: 20μm
1111
1112
1113

1114 **SUPPLMENTARY MATERIALS (Grove et al.)**

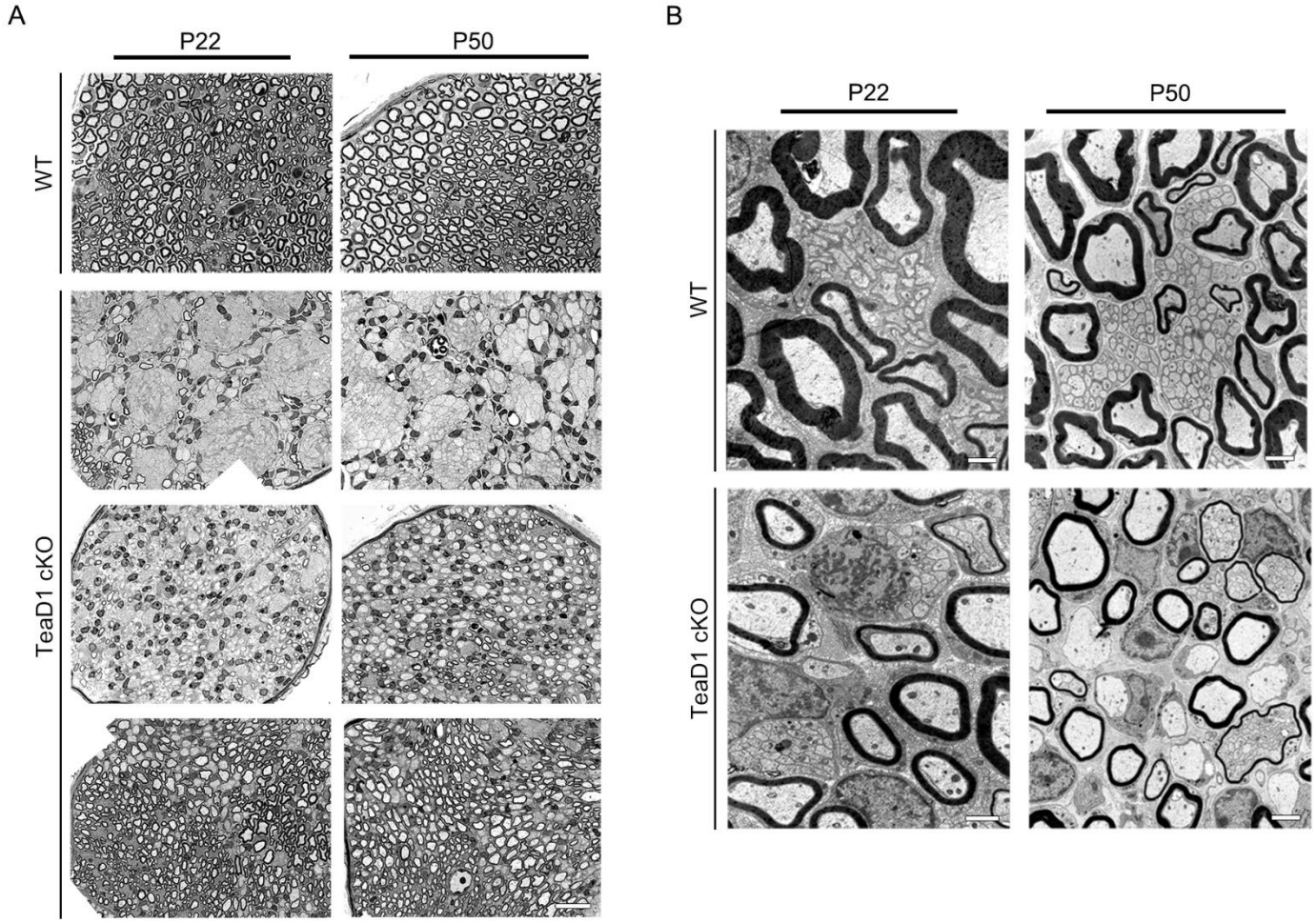

1115 **Supplementary figure 1. Additional semi-thin and TEM images of WT and *Tead1* cKO**

1116 **(A)** Representative images of semi-thin sections of various areas of WT and Tead1 cKO SNs at

1117 P22 and P50. Scale bar: 20µm

1118 **(B)** Representative TEM images of transverse sections of WT and Tead1 cKO SNs at P22 and

1119 P50. Scale bar: 1µm (P22 panels), 2µm (P50 panels)

1120

1121 **Supplementary video 1. A movie showing a P55 WT and two littermates *Tead1* cKO mice**

ACKNOWLEDGMENTS

We thank members of the Son laboratory for critical reading of the manuscript. We thank Dr. Eric Olson for *Yap* and *Taz* floxed mice, Drs. Ueli Suter and Kelly Monk for Plp-creERT2 mice. Plp-creERT2 mice were generated by Dr. Ueli Suter using a patented Cre-ERT2 construct developed by Dr. Pierre Chambon at GIE-CERBM.

FUNDINGS

This work was supported by grants from Shriners Children's (#84050 to Y-J.S.) and NIH NINDS (NS105796 to Y-J.S.).

AUTHOR CONTRIBUTIONS

Conceptualization: MG, YS
Methodology: GH, JZ
Investigation: MG, HK, SP, JA, ML, YS
Funding acquisition: YS
Supervision: ML, YS
Writing – original draft: MG
Writing – review & editing: YS

COMPETING INTERESTS

The authors declare no competing interests.

DATA AND MATERIALS AVAILABILITY

All data are available in the main text or the supplementary materials.